Hydraulic-Mechanical (HM) Numerical Modelling of Triaxial Tests of Unsaturated Clay-Based Sealing Material Using Three Computer Codes

NWMO TR-2009-34   **December 2009**

D.G. Priyanto and D.A. Dixon

Atomic Energy of Canada Limited

Nuclear Waste Management Organization
22 St. Clair Avenue East, 6th Floor
Toronto, Ontario
M4T 2S3
Canada

Tel: 416-934-9814
Web: www.nwmo.ca

Hydraulic-Mechanical (HM) Numerical Modelling of Triaxial Tests of Unsaturated Clay-Based Sealing Material Using Three Computer Codes

NWMO TR-2009-34

December 2009

D.G. Priyanto and D.A. Dixon
Atomic Energy of Canada Limited

Disclaimer:

ABSTRACT

Title: **Hydraulic-Mechanical (HM) Numerical Modelling of Triaxial Tests of Unsaturated Clay-Based Sealing Material Using Three Computer Codes**
Report No.: **NWMO TR-2009-34**
Author(s): D.G. Priyanto and D.A. Dixon
Company: Atomic Energy of Canada Limited
Date: December 2009

Abstract

This document discusses numerical modelling of the hydraulic-mechanical (HM) behaviour of unsaturated clay-based sealing material. This study focused on the behaviour of compacted Bentonite-Sand Buffer (BSB) due to extensive data base to support assessment of rigorous HM constitutive models. The BSB is a 50:50 mixture (by dry mass) of bentonite and well-graded silica sand compacted at high dry density of approximately 1.67 Mg/m^3. The objectives of this document are to: (1) calibrate the parameters of HM constitutive models; (2) apply these HM constitutive models in three different computer codes and evaluate the simulation results.

In order to achieve the first objective, this document reviewed the existing HM constitutive models. These models included: the van Genuchten (1980) and Kozeny's models to simulate the hydraulic behaviour and the Basic Barcelona Model (BBM) (Alonso et al. 1990) to simulate mechanical behaviour. The parameters of these models are calibrated based on the laboratory test results. During the calibration process, some features observed in the laboratory tests cannot be simulated using the existing HM constitutive models. Modifications of these existing constitutive models generate new constitutive models to simulate the unsaturated BSB. This document introduced three new constitutive models, including: the BBM-mod, the BSB, and the Smax models. The BBM-mod had similar features as the original BBM (Alonso et al. 1990), but it used Bishop's effective stress. The BSB model modified the volumetric change and yield functions of the BBM based on the laboratory test results of the BSB specimens. The Smax model incorporated the relationship of maximum gravimetric water content and total porosity observed at the end of the infiltration tests of the BSB specimens.

In order to achieve the second objective, these different constitutive models are implemented in three computer codes (i.e., CODE_BRIGHT, FLAC, and COMSOL). These codes are then used to simulate the HM behaviour of the infiltration process of the compacted BSB triaxial specimens in constant volume (CV) and constant mean stress (CMS) tests. The results of simulations are presented and discussed to examine the effects of each constitutive model features and formulations on the results of the HM analyses.

TABLE OF CONTENTS

TABLE OF CONTENTS (concluded)

LIST OF TABLES

Page

LIST OF FIGURES

Page

LIST OF FIGURES (concluded)

1. INTRODUCTION

The characterization of the hydraulic and mechanical (HM) behaviour of clay-based sealing material is important in assessing the overall design of a Deep Geological Repository (DGR). In the current Canadian DGR conceptual designs, the used nuclear fuel is encased in long-lived containers and surrounded by sealing materials in rooms or in borehole drilled from rooms excavated at an appropriate depth in a suitable geological media. The clay-based sealing components will initially be unsaturated. One of the clay based sealing-system components previously considered for use in a Canadian DGR is compacted Bentonite-Sand Buffer (BSB) material (Russell and Simmons 2003, Gierszewski et al. 2004; Maak and Simmons 2005). The BSB is a 50:50 mixture (by dry mass) of bentonite clay and well-graded silica sand compacted at a high dry density of approximately 1.67 Mg/m^3. Tests on the BSB have been performed at various laboratories under both saturated and unsaturated conditions (e.g., Dixon 1995, Wiebe 1996, Tang 1999, Blatz 2000, Anderson 2003, Siemens 2006, Baumgartner et al. 2008, and Priyanto et al. 2008a, 2008b). The BSB has been the focus of this study due to the extensive data base to support assessment of rigorous HM constitutive models.

The objectives of this document are to: (1) calibrate the parameters of HM constitutive models based on these laboratory test results; and (2) apply these HM constitutive models in different computer codes and evaluate the simulation results.

In order to achieve the first objective, this document reviews the existing HM constitutive models. These models include: the van Genuchten (1980) and Kozeny's models that simulate the hydraulic behaviour and the Basic Barcelona Model (BBM) (Alonso et al. 1990) to simulate the mechanical behaviour. The parameters of these models are then calibrated based on the laboratory test results.

During the calibration process, some features observed in the laboratory tests cannot be simulated using the existing HM constitutive models. Modifications of these existing constitutive models generate new constitutive models to simulate the unsaturated BSB. This document introduces three new constitutive models, including: the BBM-mod, the BSB, and the Smax models. The BBM-mod has similar features as the BBM, but different stress state variable. The BSB model modifies the volumetric change and yield functions in the BBM based on the laboratory test results of the BSB specimens. The Smax model incorporates the relationship of maximum gravimetric water content and total porosity observed at the end of the infiltration tests of the BSB specimens (Siemens 2006).

In order to achieve the second objective, these different constitutive models are implemented in three computer codes (i.e., CODE_BRIGHT, FLAC, and COMSOL). These codes are then used to simulate the HM behaviour of the infiltration process of the compacted BSB triaxial specimens in constant volume (CV) and constant mean stress (CMS) tests. The results of simulations are presented and discussed to examine the effects of each constitutive model features and formulations on the results of the HM analyses.

2. EXISTING CONSTITUTIVE MODELS

Hydraulic (H) and Mechanical (M) constitutive models are required to simulate the HM behaviour of the BSB. The existing HM constitutive models used in the analyses are the van

Genuchten (1980) and Kozeny's models to simulate hydraulic behaviour and the Basic Barcelona Model (BBM) to simulate mechanical behaviour.

2.1 HYDRAULIC CONSTITUTIVE MODELS

The hydraulic constitutive models to simulate the unsaturated clay-based sealing materials are the Soil Water Characteristic Curve (SWCC) and the permeability model. The SWCC defines the relationship of suction (s) as a function of degree of saturation (S_w), while permeability function defines the relationship of permeability (k_w) and degree of saturation (S_w) and porosity (n).

The SWCC equations based on the van Genuchten (1980) model are as follows.

$$s = P_0\left(S_e^{-1/a} - 1\right)^{1-a} \tag{1}$$

$$s = u_a - u_w \tag{2}$$

where P_o and a are constant parameters, u_a and u_w are pore air and water pressure, respectively; and S_e is the effective degree of saturation, which is defined as follows.

$$S_e = \frac{S_w - S_{res}}{S_{max} - S_{res}} \tag{3}$$

where S_{res} is the residual degree of saturation, and S_{max} is the maximum degree of saturation measured in the specimen (≤1).

Permeability functions of water (i.e., wetting fluid) and air (i.e., nonwetting fluid) used in these analyses are based on the van Genuchten (1980) model. Water (k_w) and air (k_a) permeability as a function of degree of saturation (S_w) are provided by the following equations.

$$k_w\left(S_w\right) = k_w^{sat} \cdot \left(S_e^b \left[1 - \left(1 - S_e^{1/a}\right)^a\right]^2 \right) \tag{4}$$

$$k_a\left(S_w\right) = k_w^{sat} \cdot \mu_{rat} \cdot \left(\left(1 - S_e\right)^c \left(1 - S_e^{1/a}\right)^{2a} \right) \tag{5}$$

a, b, and c are the fitting parameters, μ_{rat} is the dynamic viscosity ratio of water to air (i.e., $\mu_{rat} = \mu_w / \mu_a$), and k_w^{sat} is the water permeability at saturated conditions.

The relationship of k_w^{sat} and total porosity (n) is defined using Kozeny's model:

$$k_w^{sat} = k_0 \frac{n^3}{\left(1-n\right)^2} \frac{\left(1-n_0\right)^2}{n_0^3} \tag{6}$$

where n_0 is the initial total porosity and k_0 is water permeability corresponds to the initial porosity.

2.2 BASIC BARCELONA MODEL (BBM) (ALONSO ET AL. 1990)

2.2.1 Stress-State Variables

An elastoplastic model is preferred to describe the mechanical behaviour of unsaturated clay-based sealing materials for the numerical modelling of the DGR, where the long-term prediction of the behaviour is necessary. The Basic Barcelona Model (BBM) (Alonso et al. 1990) is used to simulate the mechanical behaviour. The BBM is the first constitutive model for unsaturated soil that was developed based on the Modified Cam-Clay (MCC) (Roscoe and Burland 1968).

At least, three combinations of independent stress-state variables are required to describe the behaviour of unsaturated compacted BSB. The BBM uses net mean stress (p), suction (s), and deviatoric stress (q). Suction is the excess of pore air pressure (u_a) over porewater pressure (u_w) (i.e., $s = u_a - u_w$). Net mean stress is the excess of mean stress (σ_m) over pore air pressure (u_a), which is:

$$p = \sigma_m - u_a \tag{7}$$

More complex stress-state variables can also be used to define the behaviour of unsaturated BSB. Application of more complex stress-state variables tends to lead to simpler constitutive equations, which can be beneficial during the implementation of the constitutive models (Sheng et al. 2008). Including degree of saturation (S_w), the Bishop's effective stress (p′) is:

$$p' = (\sigma_m - u_a) + S_w(u_a - u_w) \tag{8}$$

Net mean stress (p) (Equation 7) is used in CODE_BRIGHT, while Bishop's effective stress (p′) (Equation 8) is used in FLAC.

2.2.2 Formulation

The original BBM (Alonso et al. 1990) used net mean stress (p), suction (s), and deviatoric stress (q) in its formulation, and specific volume (v) as stress-strain variables. Figures 1 and 2 illustrate the yield surface of the BBM in p-q-s space and stress-volume surface in the p-s-v space, respectively. The equations to construct these p-q-s-v spaces are summarized as follows.

Equation to generate LC-Line (Figure 1b):

$$\left(\frac{p_o}{p_c}\right) = \left(\frac{p_o{}^*}{p_c}\right)^{[\lambda(0)-\kappa]/[\lambda(s)-\kappa]} \tag{9}$$

Stiffness parameter for changes in p for virgin state of the soil ($\lambda(s)$) is a function of s as follows.

$$\lambda(s) = \lambda(0)\left[(1-r)\exp(-\beta s) + r\right] \tag{10}$$

SI-line in Figure 1b is:

$s = s_0$ (11)

Cohesion line (ps line in Figure 1b):

$$p = -p_s = -k \cdot s \tag{12}$$

The equation for the yield ellipse is (Figure 1a):

$$q^2 - M^2(p + p_s)(p_o - p) = 0 \tag{13}$$

Stress-volume relationship (Figure 2),
- during loading-reloading at constant s within elastic range is:

$$dv = -\kappa \frac{dp}{p} \tag{14}$$

- during loading at constant s outside elastic range is:

$$dv = -\lambda(s) \frac{dp}{p} \tag{15}$$

- for drying-wetting within elastic range at constant p is:

$$dv = -\kappa_s \frac{ds}{(s + p_{at})} \tag{16}$$

- for drying outside elastic range at constant p is:

$$dv = -\lambda_s \frac{ds}{(s + p_{at})} \tag{17}$$

where;

p	is current net mean stress
p_{at}	is atmospheric pressure (~ 0.101 MPa)
p_o	is preconsolidation stress at current suction
p_o^*	is preconsolidation stress at saturated condition (s = 0)
p_c	is reference stress
M	is slope of critical state line
r	is parameter defining maximum soil stiffness
k	is parameter describing the increase of cohesion with suction
v	is specific volume
β	is parameter controlling the rate of increase of soil stiffness with suction
κ	is slope of the ln (p)-v within elastic range for constant s
κ_s	is slope of the ln (s)-v within elastic range for constant p
$\lambda(s)$	is slope of the ln (p)-v outside the elastic range for constant s
λ_s	is slope of the ln (s)-v outside elastic range for constant p
s_0	is initial SI-yield line
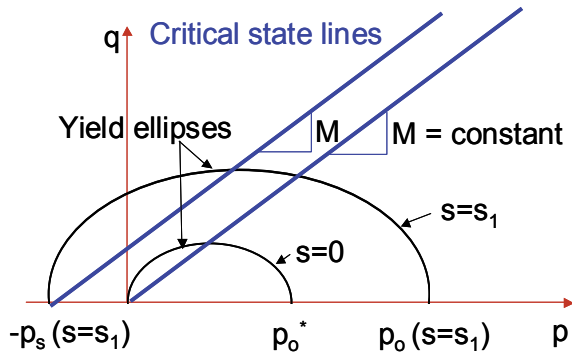
(a) p-q space
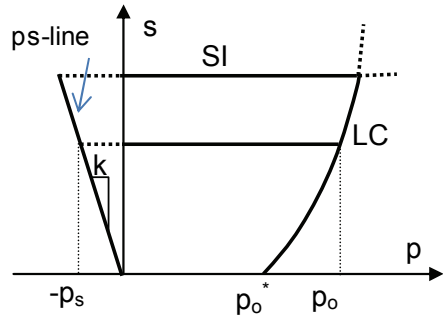
(b) p-s space
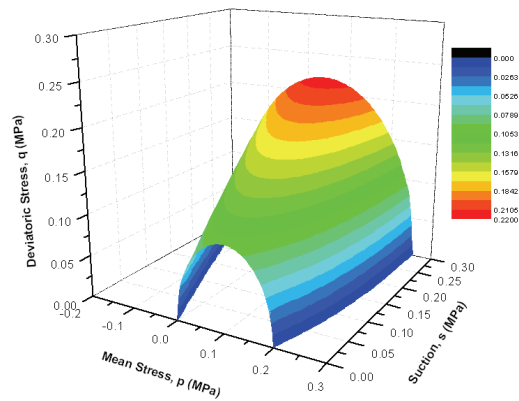
(c) p-q-s space

Figure 1: Yield Surface in p, q, s Space for the BBM

(a) ln p-v Space

(b) ln s – v Space
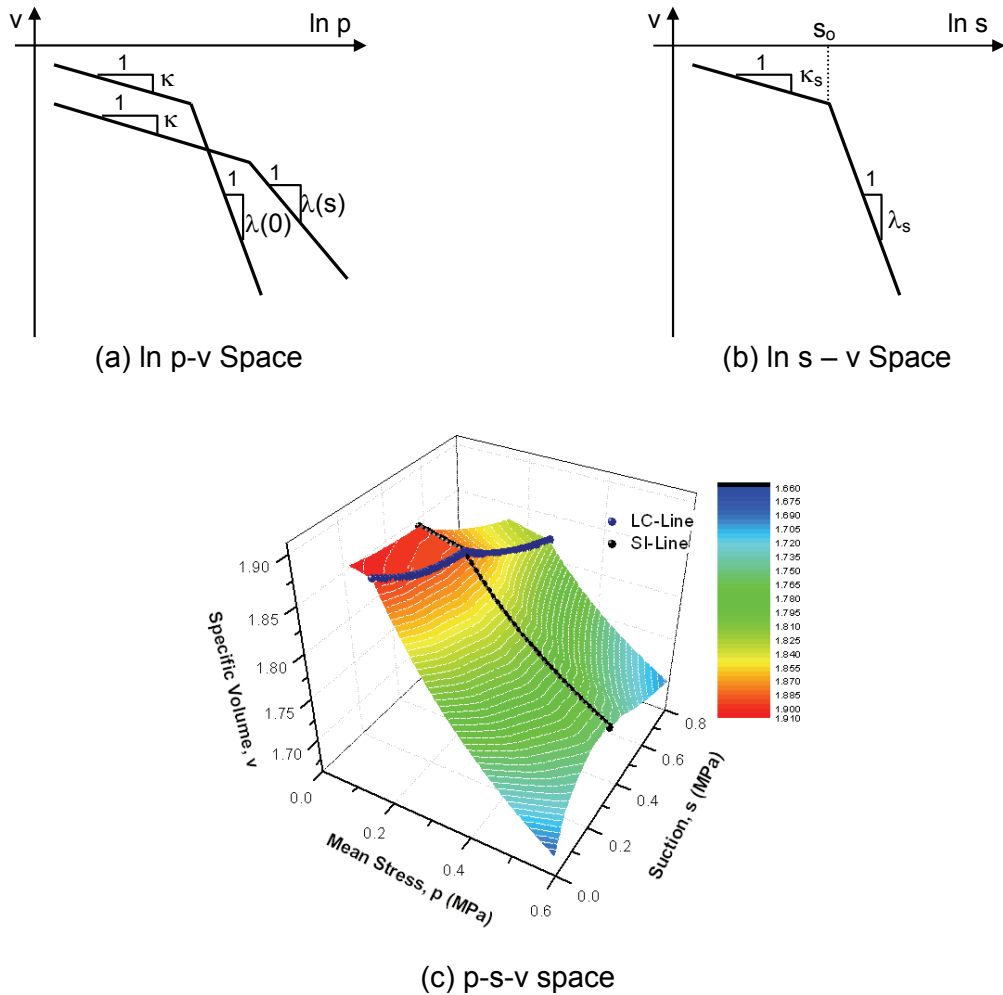
(c) p-s-v space

Figure 2: Stress-Volume Relationship in p, s, v Space for the BBM

3. CALIBRATION

3.1 CALIBRATION OF HYDRAULIC CONSTITUTIVE MODEL

3.1.1 Soil Water Characteristic Curve (SWCC)

The SWCC describes the relationship of the degree of saturation (S_w) and suction (s). Figure 3 shows the S_w-s relationships of the BSB obtained from shrinkage tests (Wiebe 1996, Tang 2000, Blatz 2000, Anderson 2003) and infiltration tests (Siemens 2006). The hysteretic behaviour of the SWCC for the BSB was observed in the drying curve obtained from the shrinkage tests and the wetting curve obtained from the infiltration test results (Figure 3). Table 1 summarizes the parameters P_o, a, S_{res}, and S_{max} to generate drying and wetting curves (Figure 3).
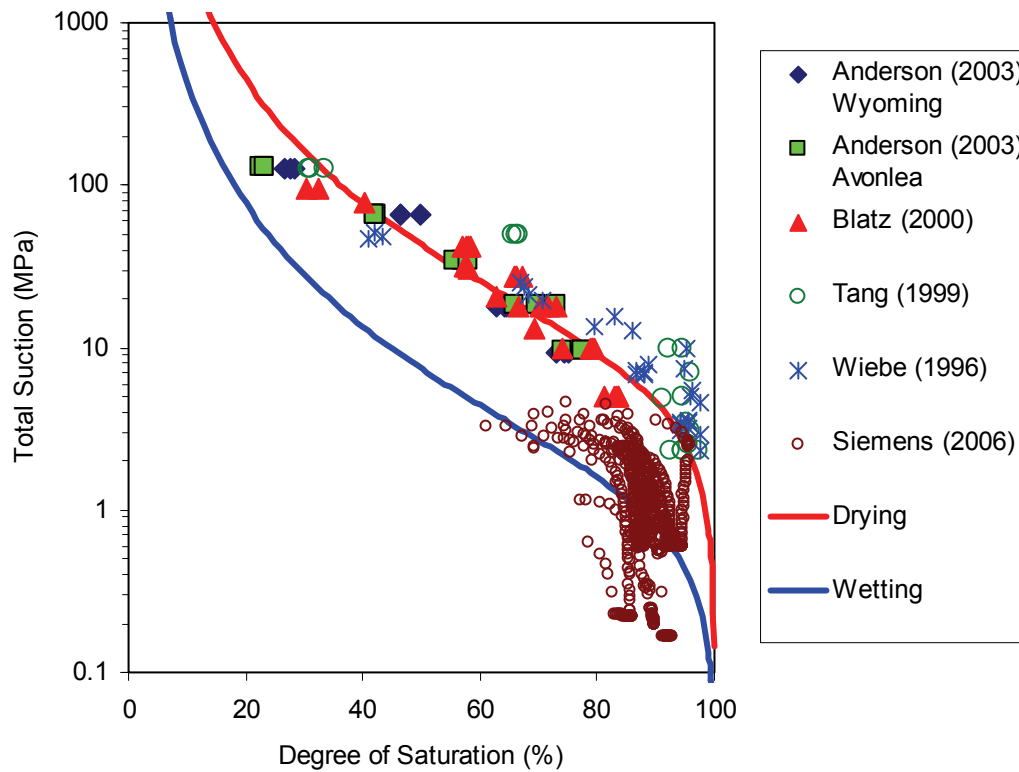
Figure 3: SWCC for the BSB Material

Table 1: SWCC Parameters for the BSB Materials

Parameters	Drying Curve	Wetting Curve
P_o (MPa)	8.01	1.37
a	0.28	0.28
S_{res} (%)	0	0
S_{max} (%)	100	100

3.1.2   Maximum Degree of Saturation (S_{max})

SWCC in Figure 3 uses van Genuchten (1980) models and assumes that the S_{max} is a constant and equal to 100% (Table 1). The infiltration test data in the S_w-s relationship shows that degree of saturation at the end of tests can be less than 100% (approximately 85 to 95%) (Siemens (2006) data points in Figure 3).

The results of the infiltration tests on the compacted BSB specimens indicated that S_{max} was dependent on the total porosity. Figure 4 shows the w_c–v relationship initial and end-of-test (EOT) data from the infiltration tests of the compacted BSB specimens (Siemens 2006). The

EOT data show a linear-relationship between gravimetric water content (w_c) and specific volume (v), which is defined by equation:

$$w_c = 37.407 \, v - 40.371 \ [\%] \tag{18}$$

Since S_w at the end of infiltration tests is equal to S_{max}, the line generated using Equation 18 is referred as Line S_{max} in Figure 4. Line S_{max} has $R^2 = 0.9801$, indicating a very good correlation to the end of test data. Line $S_{100\%}$ corresponds w_c-v relationship when $S_w = 100\%$ is also shown in Figure 4. Line $S_{100\%}$ is calculated using equation: $w_c = (v - 1)/ G_s$, where G_s is the specific gravity and equal to 2.7. Comparison of Line S_{max} and $S_{100\%}$ shows that S_{max} is less than 100% and dependent on v.

From Figure 4, S_{max} and porosity (n) can be calculated using the following equations:

$$S_{max} = w_{c\text{-}max} \cdot G_s / (v - 1) \tag{19}$$

$$n = (v-1)/v \tag{20}$$

where $w_{c\text{-}max}$ is the maximum gravimetric water content calculated from Equation 18.

This study introduces the application of the S_{max}-n relationship (Figure 4) to simulate the BSB specimen. This model is referred as Smax model and implemented in COMSOL.
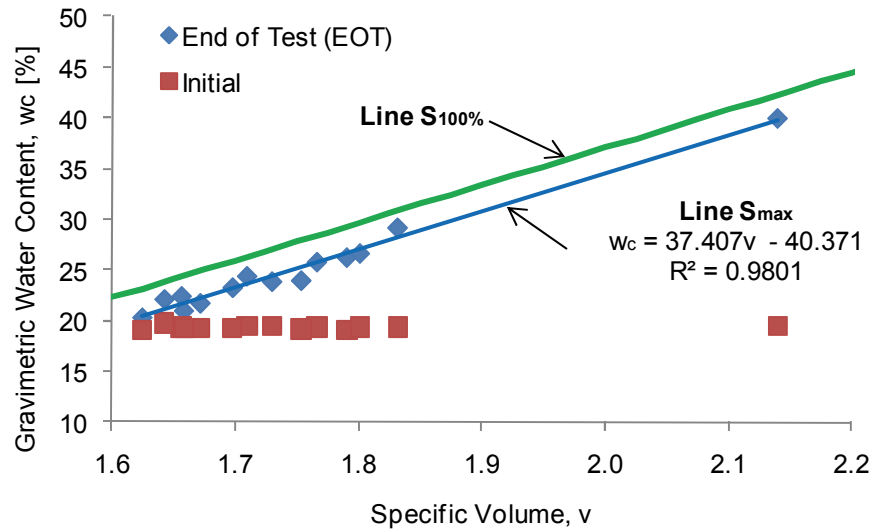
Figure 4: Gravimetric Water Content versus Specific Volume at Initial and End of Test (EOT) Observed from Infiltration Tests (data after Siemens 2006)
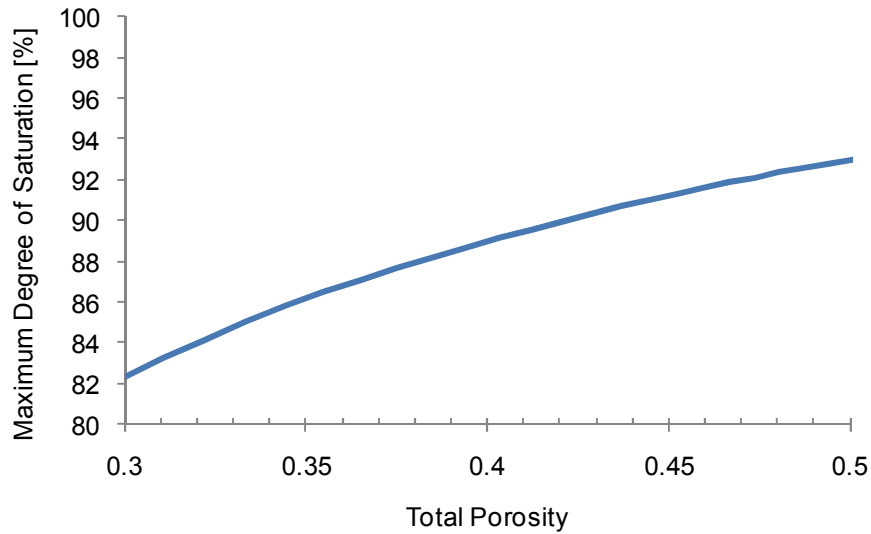
Figure 5: Maximum Degree of Saturation versus Porosity at the End of Test (EOT)

3.1.3   Permeability Function

Figure 6 shows saturated water permeability of 50:50 bentonite-sand mixture (similar composition to the BSB) from permeability tests (Dixon 1995) and one-dimensional consolidation tests (Priyanto et al. 2008). The best-fitted exponential relationship from these data is:

$$k_w^{sat} = 3 \cdot 10^{-15} \cdot e^{13.41 \, n} \, [m/s] \tag{21}$$

Substitution of the initial porosity (n) of 0.42 for the BSB in Equation 21 results in the saturated water permeability corresponding to this porosity of 8.4 x 10^{-13} m/s. Substitution of the k_0 of 8.4x10^{13} m/s and n_0 of 0.42 in Kozeny's model (Equation 6) results in saturated water permeability shown in Figure 6. This Kozeny's model, which matches the laboratory test data, is used in the simulation.

The water and air permeability during unsaturated conditions are calculated using Equations 4 and 5 with the following parameters (i.e., a = 0.28 similar to the SWCC in Table 1; b = c = 0.5).
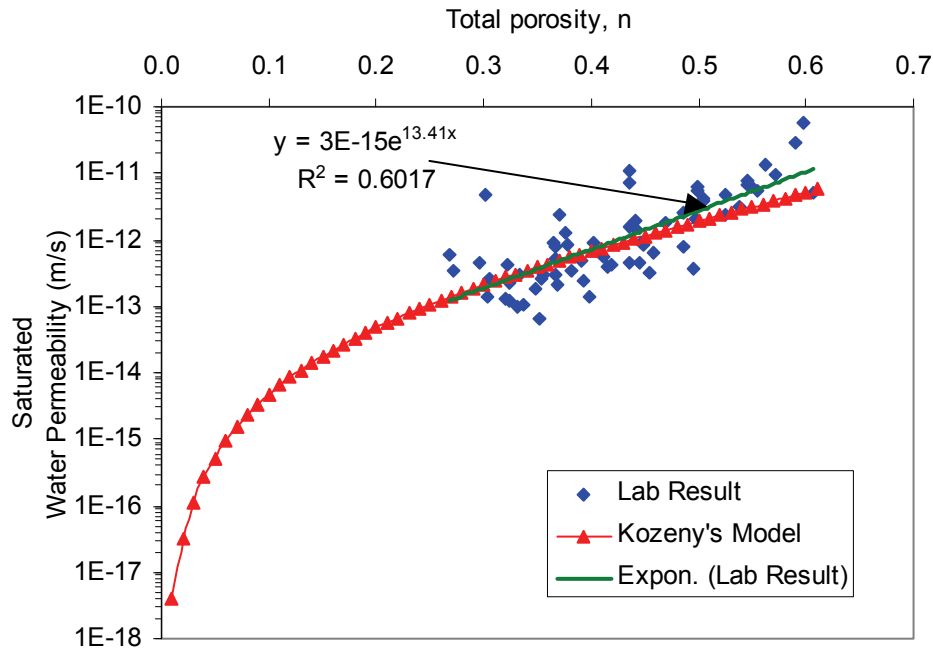
Figure 6: Saturated Water Permeability of 50:50 Bentonite-Sand Mixture

3.2   CALIBRATION OF MECHANICAL CONSTITUTIVE MODEL

The BBM parameters are calibrated using various tests on the compacted BSB materials, including: shrinkage tests and triaxial tests under isotropic loading-unloading and shearing.

3.2.1   Shrinkage Tests to Define s-v Relationship

The shrinkage tests used to define the SWCC (i.e., suction (s) - degree of saturation (S_w) relationship) can also be used to define the suction (s) - volume (v) relationship.

In the shrinkage tests (Blatz 2000, Anderson 2002, Tang 1999), immediately following compaction, the mass and dimensions of all specimens were recorded before placing them in the relative humidity (suction) environments. The ionic solutions were contained in sealed glass desiccators where a perforated plate was located above the ionic solution. During drying in the suction environments, water was drawn from the specimens to the vapour environment where it was then transferred to the ionic solution. With the increase in water content in the ionic solution, the concentration of the solution was reduced, thereby reducing the applied suction. A formula was developed to recalculate the final suction in the desiccators to take into account this mass balance consideration. Following removal of the specimens after equilibration (30 days) in the desiccators (Tang 1999), the mass and dimensions were measured again prior to placement in the triaxial cell to conduct isotropic loading-unloading and shearing tests.

During the shrinkage test, S_w decreased and s increased, while no stress was applied to the specimen. Mean stress (p) was constant and equal to zero (p~ 0). Figure 7a illustrates the results of the tests in s-v space. Plot of this test in ln(s)-v space indicates that suction increase results in the decrease of v up to suction of ~ 30 MPa (Figure 7b).

Parameter κ_s, defining the stiffness parameter due to the suction changes, can be defined from the slope of ln (s)-v and it is equal to ~ 0.65. For the BSB material, when suction is greater than ~ 30 MPa, the slope ln (s)-v decreases to almost zero indicating no volume change. This is different from the ln (s)-v relationship of the BBM (Figure 2b) featuring collapsible behaviour with an increase of suction. However, this relationship can still be defined using the BBM by setting λ_s (~ 0), and parameter s_0 ~ 30 MPa.

(a)

(b)

Figure 7: Results of Shrinkage Tests in s-v Space

3.2.2   Isotropic Loading-Unloading Under Constant Mass Condition

3.2.2.1 Description of the Laboratory Tests

Blatz (2000) and Anderson (2003) completed isotropic compression tests under constant mass condition using triaxial test with controlled suction equipment developed by Blatz and Graham (2000). Figure 8 illustrates stress paths during these tests. Initially, the BSB specimens were compacted to the target dry density and gravimetric water content of ~ 1.67 Mg/m^3 and 18.75%, respectively.

These specimens were transferred to the desiccators to achieve target suctions in the range of ~ 5 to 125 MPa (path A-B in Figure 8) before isotropic loading-unloading were applied to the specimen using triaxial test equipments (path B-C-D in Figure 8). Total masses of specimens and gravimetric water content are constant during these loading-unloading processes (B-C-D). Blatz (2000) measured the suction using psychrometer embedded within the specimens and showed that during isotropic loading, suction changed with relationship of $\Delta s/\Delta p$ ~ -0.83. Anderson (2003) did not measure suction (s) during the isotropic loading unloading, but this $\Delta s/\Delta p$ relationship was used to define suction during isotropic compressions.

A-B: Drying in desicator
B-C-D : Isotropic loading-unloading
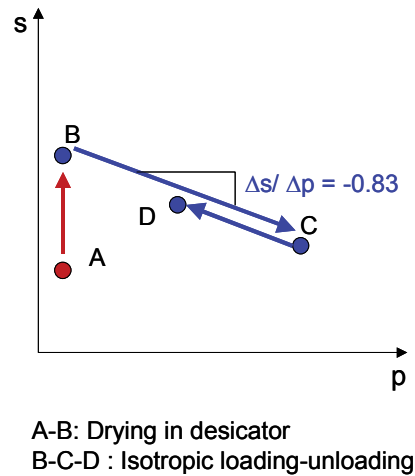
Figure 8: Stress Path in p-s Space (q = 0)

3.2.2.2 Distributions of Parameters p_o, κ, and $\lambda(s)$ with Suction from Individual Test

Figure 9 shows one of the results of isotropic loading in p-v space (i.e., specimen DA-007 (Anderson 2003)). A number of similar types of tests for different suction levels have been completed on compacted BSB triaxial specimens (Blatz 2000, Anderson 2003).

The method used to determine the parameters p_o, κ, and $\lambda(s)$ from the results of each test is described as follows. Plots of ln(p) versus v are created from the laboratory test results. Two log-linear lines (B-po and po-C in Figure 9) created on this plot. The intersection between these two lines is equal to the preconsolidation pressure at the corresponding suction (p_o).

Total volume change during the isotropic compression is the summation of volume changes due to mean stress changes (dp) and suction changes (ds).

Within elastic range ($p < p_o$ and $s < s_0$), total volume is:

$$v = v_{in} + \kappa \ln\left(\frac{p}{p_{in}}\right) + \kappa_s \ln\left(\frac{s}{s_{in} + p_{at}}\right)$$ (22)

Where p_{in}, v_{in} and s_{in} represent the initial state.

Outside elastic range ($p > p_o$ and $s < s_0$):

$$v = v_{in} + \kappa \ln\left(\frac{p_o}{p_{in}}\right) + \lambda(s)\ln\left(\frac{p_o}{p_{in}}\right) + \kappa_s \ln\left(\frac{s}{s_{in} + p_{at}}\right)$$ (23)

For $s > s_0$, κ_s in Equations 22 and 23 are substituted with λ_s.

Parameters κ_s, λ_s, and s_0 have been determined from the result of shrinkage test previously, where $\kappa_s \approx 0.65$, $\lambda_s \approx 0$, and $s_0 \approx 30$ MPa, while p_o are determined graphically (Figure 9).

Substitutions of these known parameters into Equations 22 and 23 result in two unknown parameters κ and $\lambda(s)$. These two parameters (κ and $\lambda(s)$) can be determined by fitting the Equations 22 and 23 to the laboratory test results. Built-in function, called 'Solver', in MS-Excel was used as a tool in this process. These processes are completed for each test (Anderson 2003, Blatz 2000). Distributions of preconsolidation pressure (p_o), parameter κ and $\lambda(s)$ with suction are illustrated in Figures 10, 11 and 12, respectively.
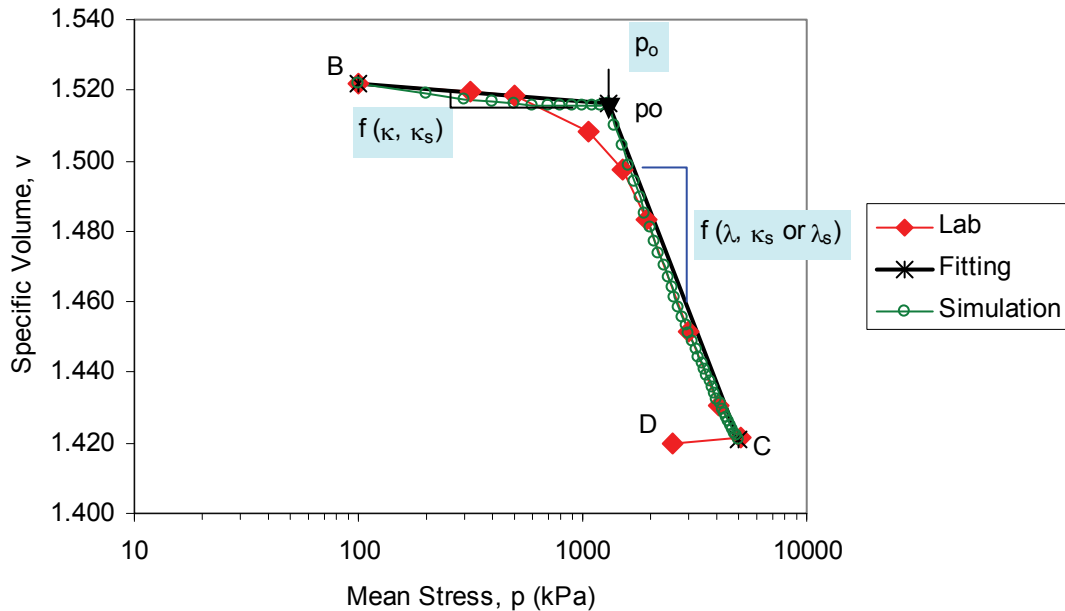
Figure 9: Results of Triaxial Tests during Isotropic Loading-Unloading (Specimen DA-007, Anderson 2003)
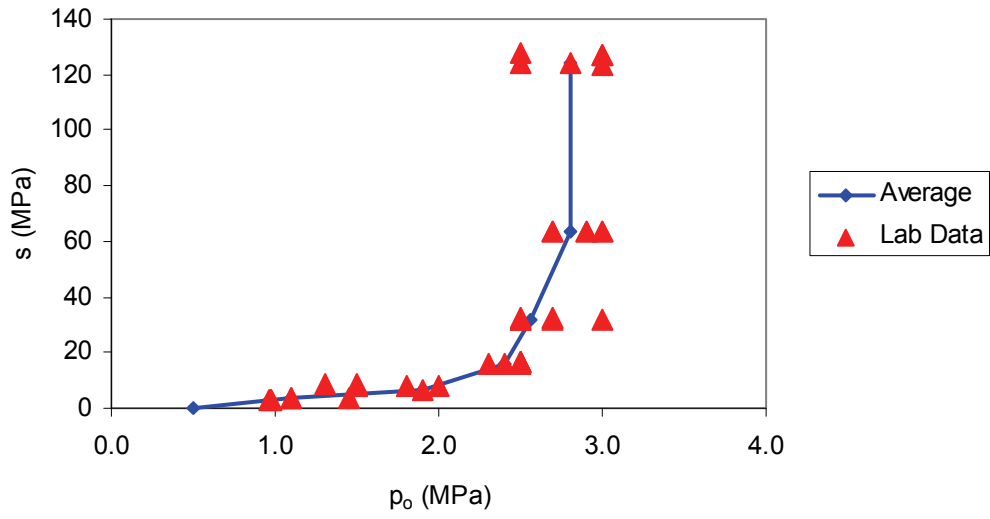
Figure 10: Preconsolidation Pressure p_o with Suction
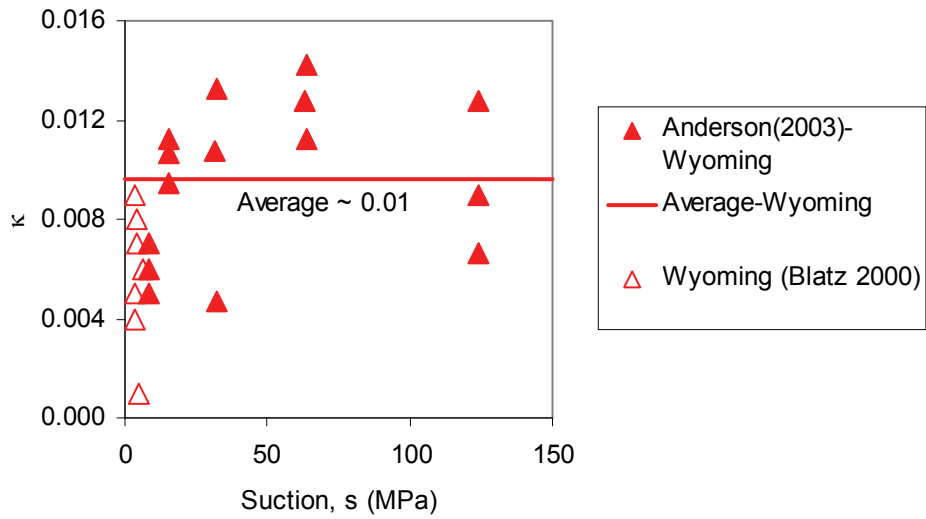
Figure 11: Distribution of Parameter κ with Suction
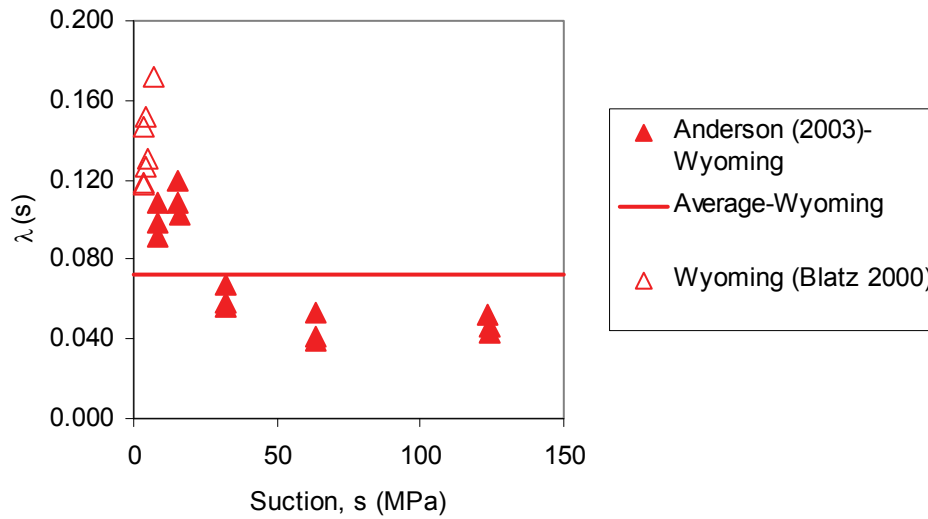
Figure 12: Distribution of Parameter λ(s) with Suction

3.2.3 Determination of the Parameters p_o, κ, and λ(s) with Suction

The results of triaxial tests on the compacted BSB specimens show that with suction increase, preconsolidation pressure (p_o) increases (Figure 10) and parameter λ(s) decreases (Figure 12), which also the characteristics of the BBM (Alonso et al. 1990). Figure 11 shows that parameter κ of the BSB increases with suction, which is not the case of the BBM where parameter κ is a constant. Parameter κ of approximately 0.01, the average value of κ in Figure 11, is used in the modelling using the BBM.

3.2.4 Determination of the Parameters Corresponding to the Yield Line

The yield line of the BBM (LC in Figure 1b) is calculated using Equations 9 and 10. In the BBM, LC line (Equation 9) is coupled with the λ(s) function (Equation 10). Parameters corresponding to this LC line and λ(s) function are p_o*, p_c, κ, λ(0), λ(s), r, and β.

At this point, parameter κ has been determined previously as equal to 0.01. Based on the laboratory tests data (Blatz 2000, Tang 1999), preconsolidation pressure at saturated condition (p_o*) is approximately 0.5 MPa. Using these known values (i.e., κ = 0.01 and p_o* = 0.5), the rest of the parameters (i.e. p_c, λ(0), r, and β) are defined by fitting Equations 9 and 10 with laboratory test data. Since Equations 9 and 10 are related, a built-in function 'solver' in MS-Excel was utilized to simultaneously fit these Equations 9 and 10 with the laboratory test data. This process results in the BBM parameters; r = 0.22, β = 0.3 MPa^{-1}, λ(0) = 0.26, p_o* = 0.5 MPa, p_c = 0.34. Substitution of these parameters into Equations 9 and 10 result in the p_o-s and λ(s)-s relationships shown in Figures 13 and 14. Comparisons of these p_o-s and λ(s)-s relationships with the results of the laboratory test data indicate that these set of BBM parameters are representative to simulate the BSB material.
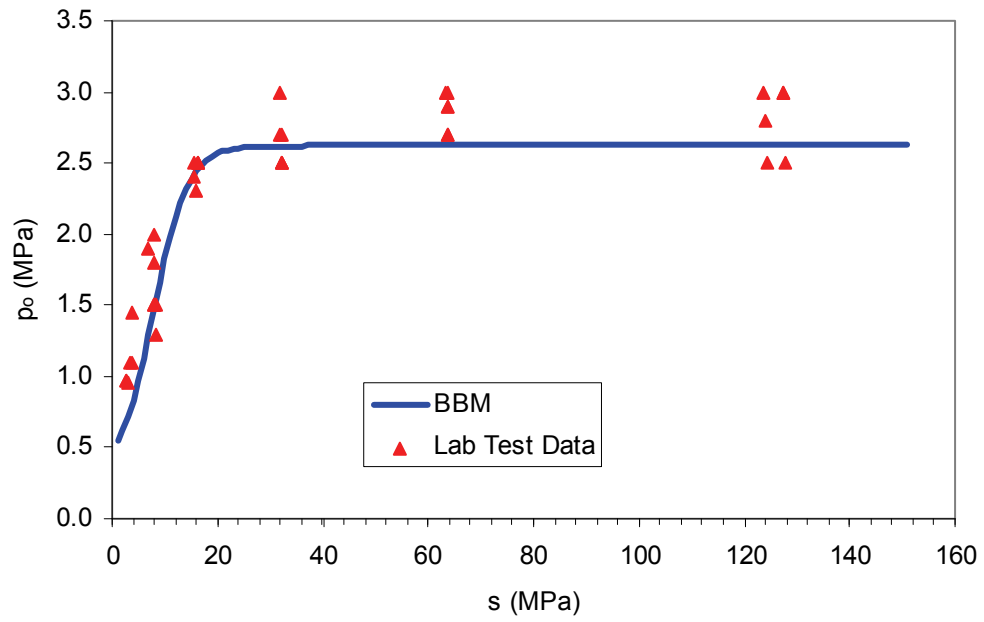
Figure 13: LC-Line of the BBM Compared to the Laboratory Test Data
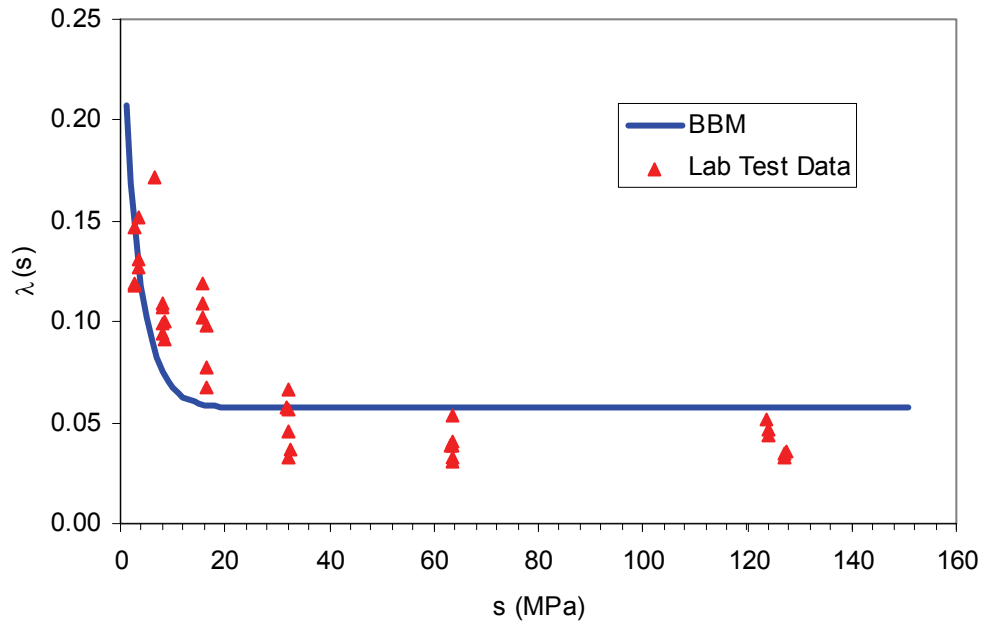
Figure 14: λ(s) of the BBM Compared to the Laboratory Test Data

3.2.5   Tensile Strength

The tensile strength for the BSB was taken from Tang (1999). In his study, the tensile strength of the BSB measured was equal to 0.31 MPa at suction of 10. For suction (s) greater than s_o (~ 30 MPa for the BSB), the preconsolidation pressure (p_c) and $\lambda(s)$ are constant with suction changes (Figures 13 and 14). Consequently, it should be similar for the tensile strength. Tensile strength of the BSB (p_s) increases with suction up to s_0 and is constant for suction greater than s_0 (Figure 15), which can be generated using the following equation.

$$p_s = -(p_{s0} + k \cdot s) \qquad \text{for } s < s_0 \tag{24a}$$

and

$$p_s = -k \cdot s_0 \qquad \text{for } s \geq s_0 \tag{24b}$$

where k = 0.21, p_{s0} = 0.1 MPa (i.e., atmospheric pressure), and s_0 = 30 MPa. Note that negative sign indicates tensile stress. Combining the LC-Line (Figure 12), SI-Line, and tensile line, the initial elastic area in the p-s space at the isotropic condition (q = 0) is illustrated in Figure 16.
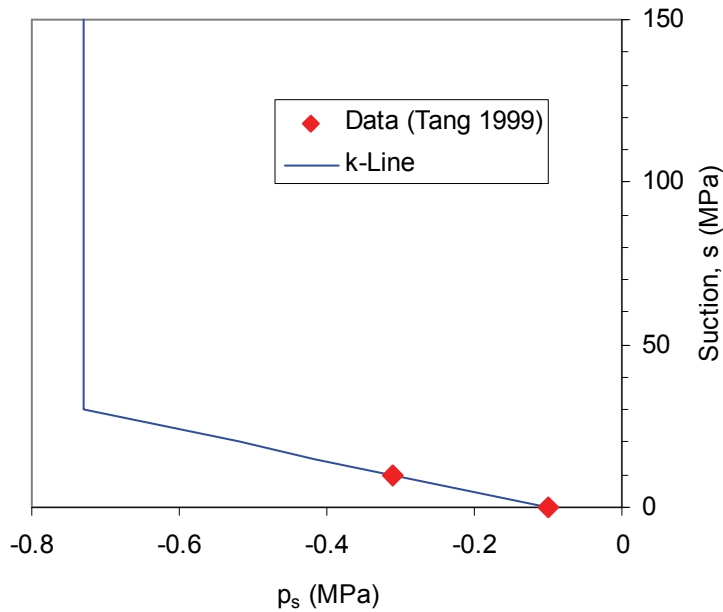
Figure 15: Tension Line
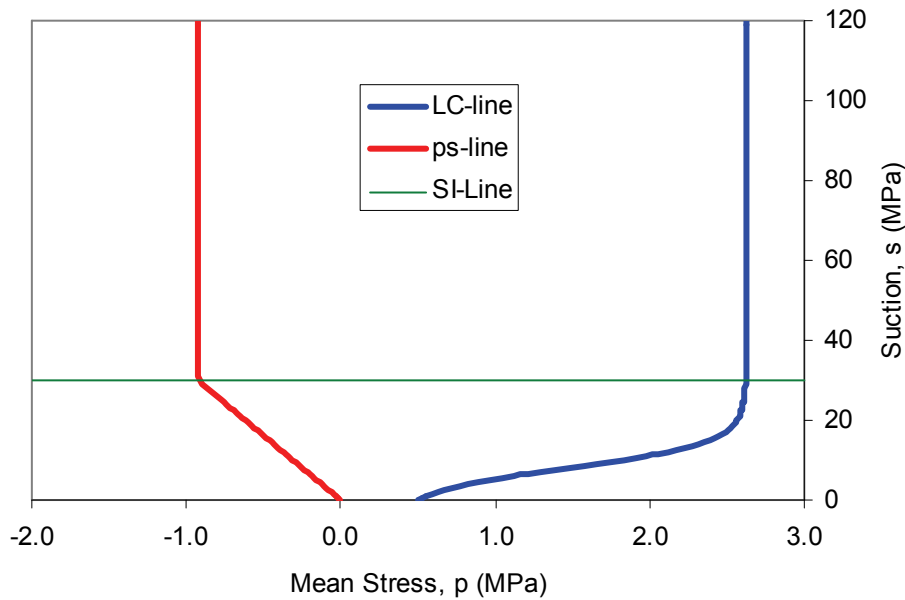
Figure 16: Yield Line at Isotropic Condition (q=0)

3.3   SHEAR STRENGTH

3.3.1   Laboratory Test Results

The parameters that define the shear strength of BSB can be interpreted from the results of the laboratory triaxial test during shearing (e.g., Anderson 2003, Blatz 2000). Following the isotropic loading-unloading (q = 0), a combination of the axial and radial stresses were applied to the specimen to follow targeted stress path in p-s space. During shearing process, the suction was constant (Blatz 2000, Anderson 2003). Figure 17a shows the two of the stress paths for specimens DA-017 and DA-018, with suction s ~ 20 MPa. Figure 17b shows the shear strain response of both specimens. Two types of behaviour can be observed (Figure 17b): ductile behaviour (strain hardening) (specimen DA-018); and brittle behaviour (strain softening) (specimen DA-017).

The BBM is based on the MCC models. The computed BBM response is shown as dashed lines in Figure 17b. For specimen DA-017, having strain softening behaviour, the peak point should be the yield point and the end of test (or large strain point) will be located on the critical state surface. For specimen DA-018, having strain hardening behaviour, the initial yield point will be located at the point where q-ε_s relationship start becoming non-linear (~ 2000 kPa, Figure 17b). This yield point increases following the strain hardening process until deviatoric stress (q) reaches the peak (Figure 17b). The peak point at the end of test should be located on the critical state surface. Figure 17a shows the yield points and critical state points of the specimens DA-017 and DA-018 in p-q space.

The yield points and critical state points of the rest of the specimens (Blatz 2000, Anderson 2003) are determined using similar methods. Figure 18 shows the critical state points in the p-q-s space. These critical state points consist of two different tests by Blatz (2000) and

Anderson (2003). Critical state surfaces for Blatz (2000) and Anderson (2003) are created using 3D-interpolation using ORIGIN Lab[1] and shown in Figures 19a and 19b, respectively. Figure 19c compares critical state surfaces from both tests.
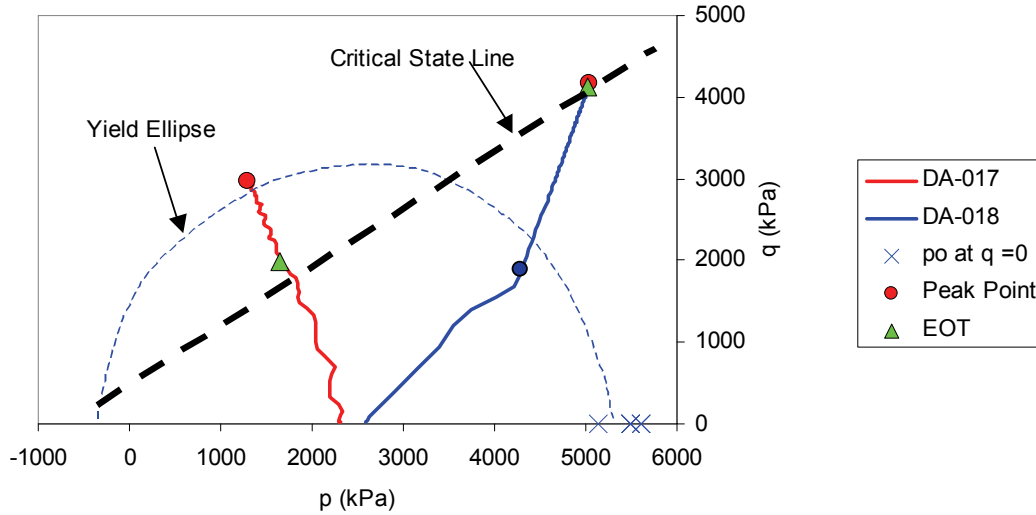
(a)
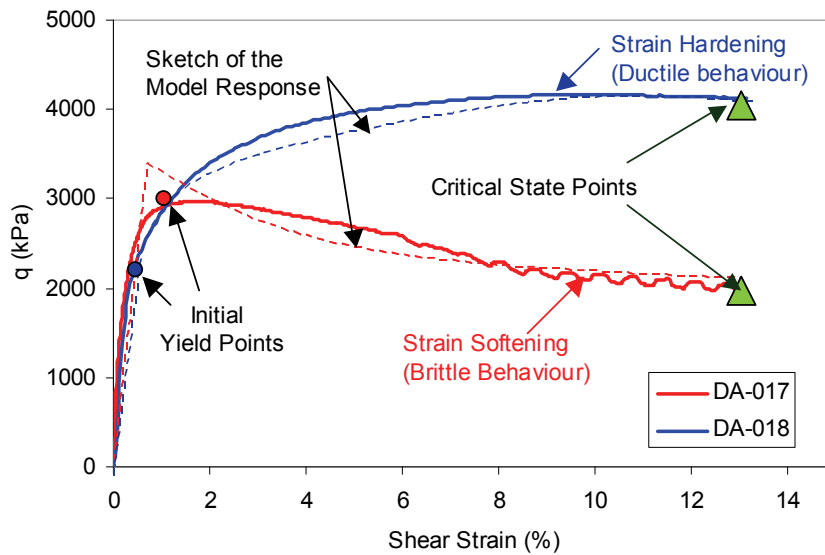
(b)

Figure 17: Results of Triaxial Tests During Shearing (s ~ 20 MPa) (data after Anderson 2003)

---

[1] OriginLab Corporation. One Roundhouse Plaza, Suite 303. Northampton, MA 01060. USA. www.OriginLab.com
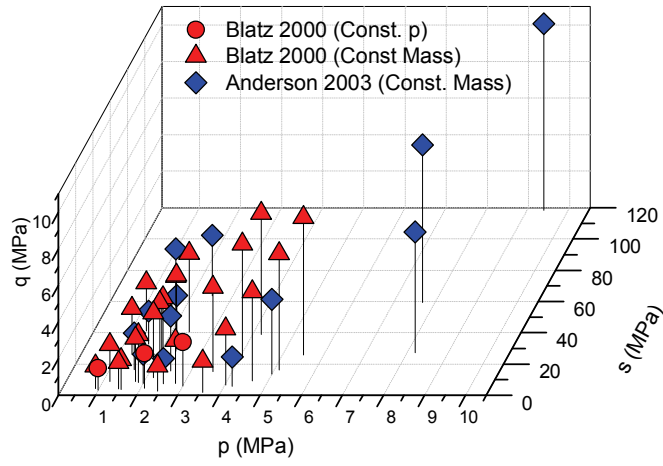
Figure 18: Critical State Points in p-q-s Space

(a)

(b)

(c)
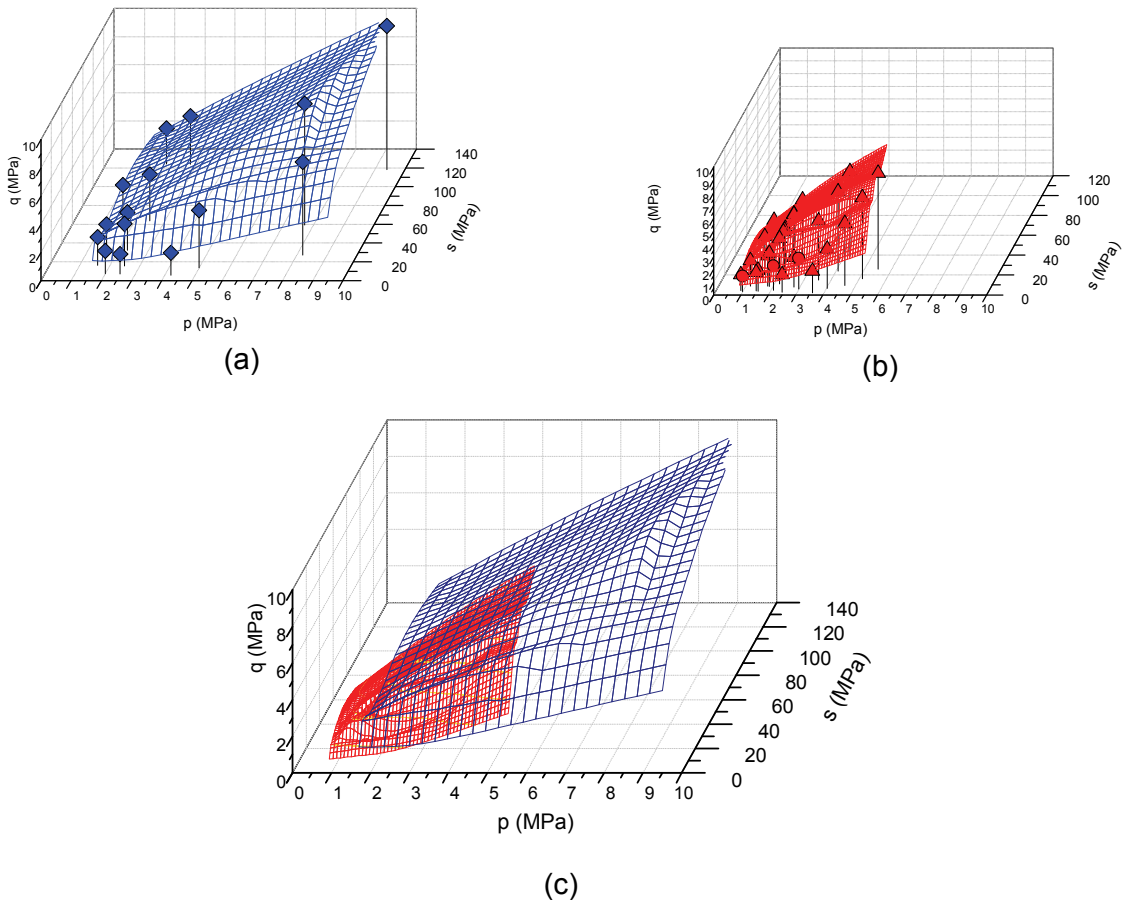
Figure 19: Critical State Surface from Laboratory Test Data

3.3.2   Determination of Critical State Surface Equation and Its Parameters

Figure 19 was created to visualize the critical state surface from laboratory test data in p-q-s space, but no equation has been determined in that process. Application of this critical state surface in a computer code requires determination of the equation of this critical state surface, and implementation of this equation in a computer code.

This section examines two possible critical state surface equations using:
- constant M, and
- M = f(s)

3.3.2.1 Critical State Surface with a Constant M

For simplicity and due to the limitation of laboratory test data, most of constitutive models (e.g., BBM or Modified Cam-Clay) assumed that the critical state line is linear with constant critical state slope (M = constant) and intersects at tension line for q=0 (Figure 1). For constant suction, the critical state slope (M) can be calculated as follows.

$$M(s) = \frac{q_{CSL}(s)}{[-p_s(s) + p_0(s)]/2} \tag{25}$$

The BBM with constant M is available in CODE_BRIGHT without requires additional development of a user-defined constitutive model and will be used to simulate the BSB.

3.3.2.2 Equation with M = f(s)

Figure 20 shows the critical state slope (M) from the results of triaxial tests. M of the compacted BSB specimens increases with s, when $s < s_0$ and M is constant when $s > s_0$, where $s_0 \sim 30$ MPa.

The slope M, as a function of s, can be defined as follows.

$$M = M_0 + k_M \cdot s \qquad \text{for } s < s_0 \tag{26a}$$

and

$$M = M_{max} \qquad \text{for } s > s_0 \tag{26b}$$

where M_0 is the critical state slope at saturation (s = 0); M_{max} is the maximum critical state slope at s_0; k_M is the changing rate of critical state slope M for $s < s_0$:

$$k_M = \frac{M_{max} - M_0}{s_0} \tag{26c}$$

The critical state surface with M=f(s) can be implemented with the development of a user-defined constitutive model in FLAC. This implementation will be discussed in section 4.4.2.

3.3.2.3 Critical State Surface Parameters

The critical state surface parameters can be determined from the triaxial test results (Figure 20). Figure 20 shows the data points of the critical state slope from the triaxial tests with different suction. Determined from these data, the parameters in Equations 26a, 26b, and 26c are $M_0 = 0.3$, $M_{max}=1.1$, and $s_0=30$ MPa, which results in a bilinear line (Figure 20). The range of critical state slope (M) from the laboratory test results is approximately 0.3 to 2 (Figure 20). A constant M of 1 is used for the whole range of suction in the analysis using the BBM.

The critical state surfaces using M=1 and M=f(s) are illustrated in Figure 21a and 21b, respectively. The critical state points from the laboratory tests are also shown in these figures. Compared to the laboratory tests data points, the critical state surface with M=1 underestimates the shear strength of the BSB for higher suction, indicated by some critical state points located below the surface (Figure 21a). The critical state surface with M=f(s) is closer to the laboratory tests data points, indicated by more points being located on the surface (Figure 21b). This comparison shows the significance of using critical state surface with M=f(s), especially when there is large suction variation.

The yield loci in p-q-s space can be created by combining: the critical state surface, the yield surface in p-s space at isotropic conditions (Figure 16) and elliptical yield locus (Figure 17a, generated using Equation 13). Figures 22a and 22b show the yield loci created using M=1 and M=f(s), respectively. These figures illustrate how the change of the critical state slope M also affects the yield loci in p-q-s space.

This section has established a method for deriving the HM properties of the unsaturated compacted BSB materials. In addition, this section also shows that a three-dimensional visualization of the constitutive models is beneficial to understand the relationship between multiple variables in order to determine these parameters. The BBM parameters for the BSB material used to generate Figures 21 and 22 are listed in Table 2.
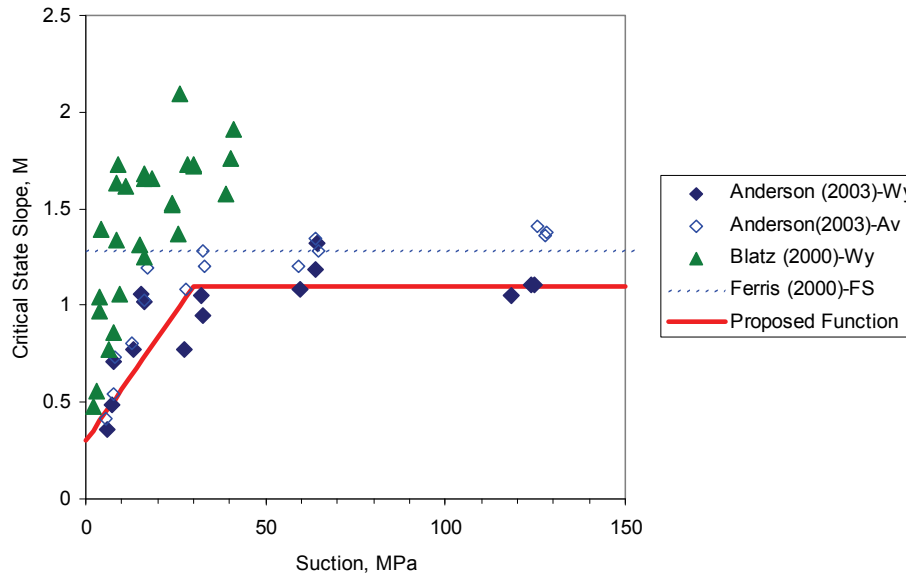
Figure 20: Critical State Slope

**Table 2: Basic Barcelona Model (BBM) Parameters for Compacted
Bentonite-Sand Buffer (BSB) Material**

Parameters	Value	Unit	Definitions
p_{at}	0.1	MPa	atmospheric pressure (~ 0.101 MPa)
$p_o{}^*$	0.5	MPa	preconsolidation stress at saturated condition (s = 0)
p_c	0.34	MPa	the reference stress
R	0.22		the parameter defining maximum soil stiffness,
K	0.021		parameter describing the increase of cohesion with suction
β	0.30	1/MPa	parameter controlling the rate of increase of soil stiffness with suction
κ	0.01		slope of the ln (p)-v within elastic range for constant s
κ_s	0.065		slope of the ln (s)-v within elastic range for constant p
λ_s	~ 0		slope of the ln (s)-v outside elastic range for constant p
p_{s0}	0.1	MPa	Tension line at suction (s = 0)
s_0	30	MPa	the initial suction increase yield line
M	1		the critical state slope (for model with constant M)
M_{max}	1.1		the maximum critical state slope (for model with M = f(s))
M_0	0.3		the critical state slope at suction = 0 (for model with M = f(s))
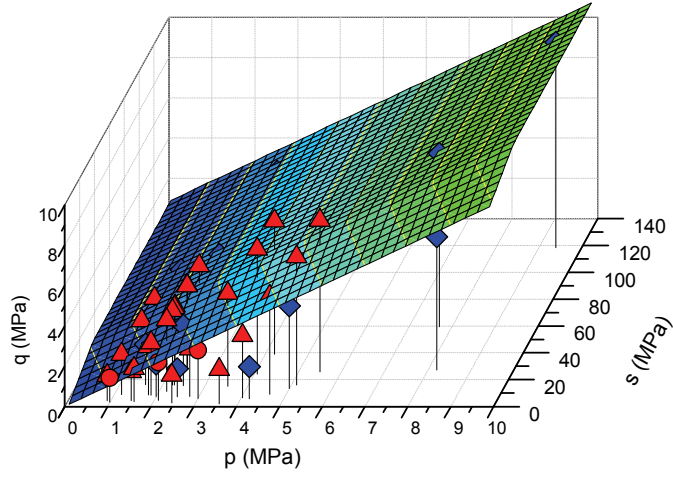
(a) M = 1
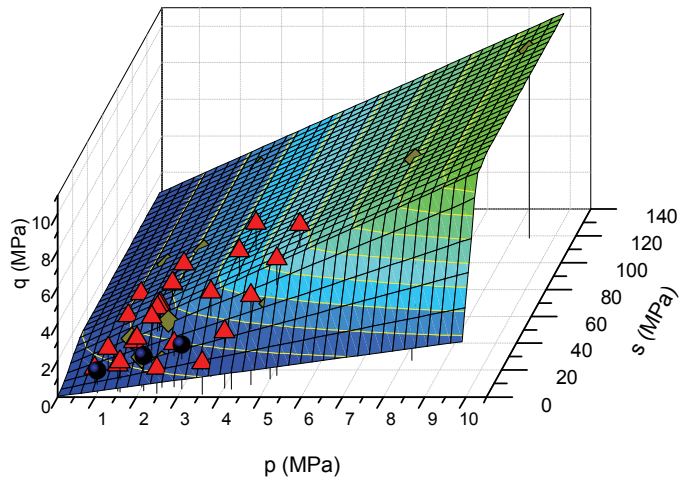
(b) M = f (s)

Figure 21: Critical State Surface of the BBM with Two Different Critical State Slope Functions
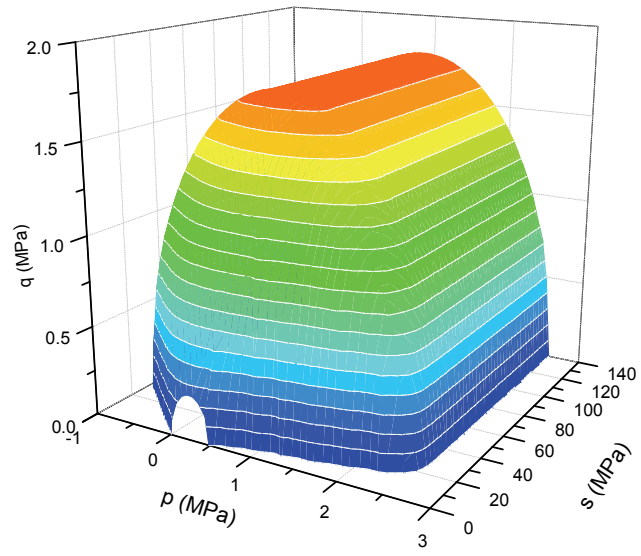
(a) M = 1
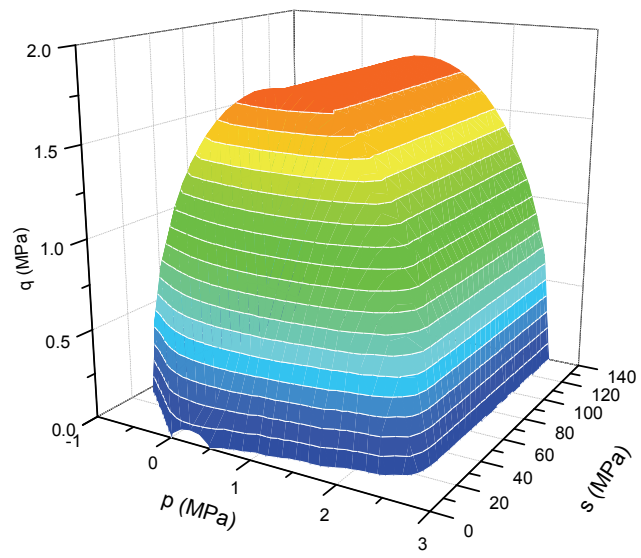
(b) M = f (s)

Figure 22: Yield Loci of the BBM with Two Different Critical State Slope Functions

4. MODELLING TRIAXIAL TESTS

4.1 TESTS DESCRIPTIONS

Two types of triaxial tests that involve infiltration into BSB specimens (Siemens 2006) are simulated using three different computer codes (i.e., CODE_BRIGHT, FLAC, and COMSOL). These tests have two different boundary conditions; constant volume (CV) and constant mean stress (CMS). The measurements during each test included: total suction; volume of water added to the specimen; radial, axial, and volume strains; and confining stress applied to the specimen. Gravimetric water content (w_c) and dry density (ρ_{dry}) were measured prior to the compaction and immediately at the end of each test. The details of the laboratory tests have been provided in the original document (Siemens 2006) and will not be repeated in this document.

Figure 23 illustrates the measurement of the volume of water added to the specimen during the conduct of the triaxial tests. Each test consisted of two stages: equilibrium and infiltration stages. In the equilibrium stage, no water was added to the specimen, while the confining pressure was increased and equilibrated. Following this stage, water was then added to the system during the infiltration stage, while axial and radial displacements and confining stress were controlled and measured. The total suction was measured during both stages.

These two stages were marked by three conditions: (1) as-compacted; (2) pre-infiltration; and (3) end of test (EOT) conditions. The gravimetric water content (w_c) and dry density (ρ_{dry}) of the specimen were measured at as-compacted and EOT conditions. The specimen was in the triaxial apparatus at pre-infiltration condition; consequently direct measurements of these properties were not possible during the intermediate stages of testing. However, they can be calculated using measurements obtained during the tests. The numerical modelling described in this document only considered the infiltration stage. Thus, the pre-infiltration condition was used as the initial condition for numerical modelling of subsequent behaviour.
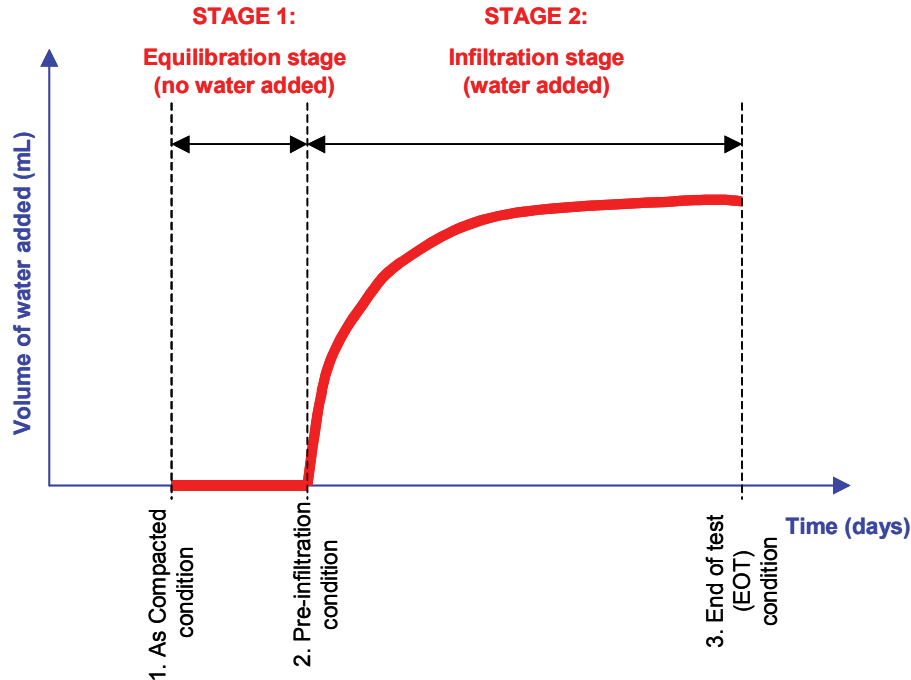
Figure 23: Definition of the Stages and Conditions of the Tests

4.2   BOUNDARY AND INITIAL CONDITIONS

Figure 24a shows the dimensions of triaxial specimen in the test. Figures 24b, 24c, and 24d show the boundary and initial conditions present in the numerical modelling of constant volume (CV) and constant mean stress (CMS) tests. The specimens have a cylindrical shape, 50 mm in diameter and 100 mm in height (Figure 24a). Due to the symmetrical shape of the triaxial specimen, only half of the specimen is simulated in the numerical models using axisymmetric geometry. Thus the numerical model simulates a radius of 25 mm and a height of 50 mm.

The hydraulic boundary and initial conditions are the same for CV and CMS tests (Figure 24b). The top of the specimen and the symmetry line are impermeable (which represents no drainage paths at those locations). A pore water pressure of 0.2 MPa is applied around the specimen perimeter during the test. The specimen initially has 18.75% gravimetric water content (corresponding to an initial degree of saturation of 70%) and atmospheric pore air pressure of approximately 0.101 MPa.

The initial mean stress of both CV and CMS tests is 0.5 MPa (Figures 24c and 24d). The mechanical boundary conditions are different for CV and CMS tests (Figures 24c and 24d). The top, symmetry line, and perimeter of the model of the CV specimens have roller mechanical boundary conditions as illustrated in Figure 24c. Application of these mechanical boundary conditions for model of the CV specimen results in constant total volume, but allows the displacement of the internal grids to investigate the variation of dry density along radial and axial direction. The confining stress of 0.5 MPa is applied around the perimeter and at the top of model of the CMS specimen (Figure 24d). Zero y-displacement is assigned at the symmetry line for CMS specimen (Figure 24d).
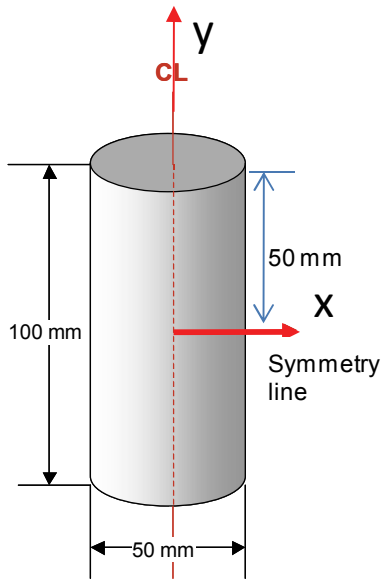
(a) Triaxial Specimen
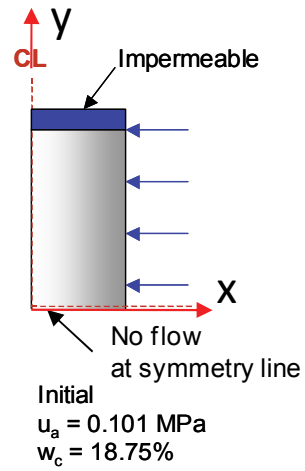
(b) Hydraulic Boundary Condition for Constant Volume (CV) and Constant Mean Stress (CMS)
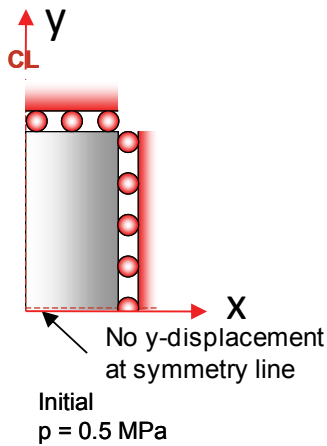
(c) Mechanical Boundary Condition of Constant Volume (CV) Test
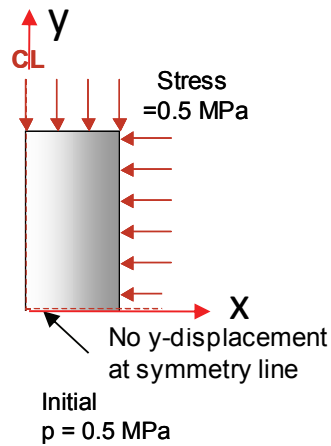
(d) Mechanical Boundary Condition of Constant Mean Stress (CMS) Test

Figure 24: Mechanical and Hydraulic Boundary Conditions

4.3 GRIDS AND BOUNDARY CONDITIONS

The elements and grids used in the analysis using CODE_BRIGHT, FLAC, and COMSOL are illustrated in Figures 25 to 27, respectively. In this study, CODE_BRIGHT analyses used 10x20 rectangular grids (Figure 25), FLAC analyses used 10x20 rectangular grids Figure 26), and COMSOL analyses used 314 Lagrange-Quadratic triangular elements (Figure 27). The boundary conditions applied to the model are also illustrated in the figures.

The analysis method, formulation used to solve HM problem, and mechanical and hydraulic constitutive models used in the analyses are summarized in Table 3. In total, eight (8) analyses were completed using three different computer codes to simulate CMS and CV tests described previously. CODE_BRIGHT and COMSOL analyses use the Finite Element Method (FEM), while FLAC models use the Finite Difference method. CODE_BRIGHT and COMSOL analyses use one-phase fluid flow formulation, assuming constant pore air pressure, while FLAC analyses use two-phase fluid flow formulation. The H-M constitutive models used in the study are as follow. CODE_BRIGHT analyses use the original BBM. FLAC analyses use two different mechanical constitutive models: BBM-mod (i.e., modified BBM model using Bishop's effective stress) and BSB model. COMSOL analyses use linear elastic model. Both CODE_BRIGHT and FLAC analyses use the van Genuchten's SWCC with constant S_{max} of 100%. COMSOL analyses use SWCC with S_{max} as a function of porosity, which will be called Smax model in this document. All analyses use Kozeny's model to describe saturated permeability.

(a) 10x20 Rectangular Elements

(b) Constant Mean Stress (CMS)

(b) Constant Volume (CV)
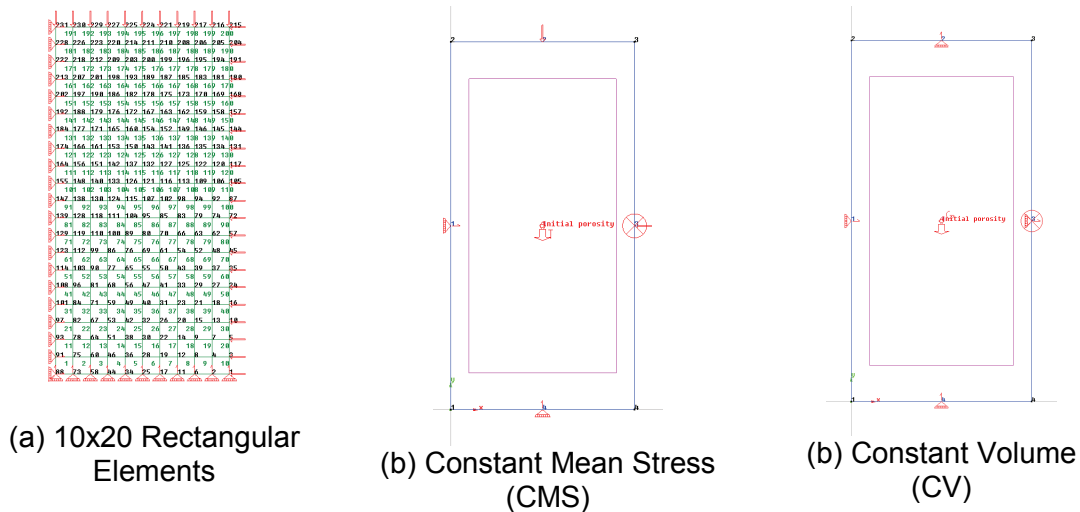
Figure 25: Elements and Boundary Conditions used for Analyses using CODE_BRIGHT
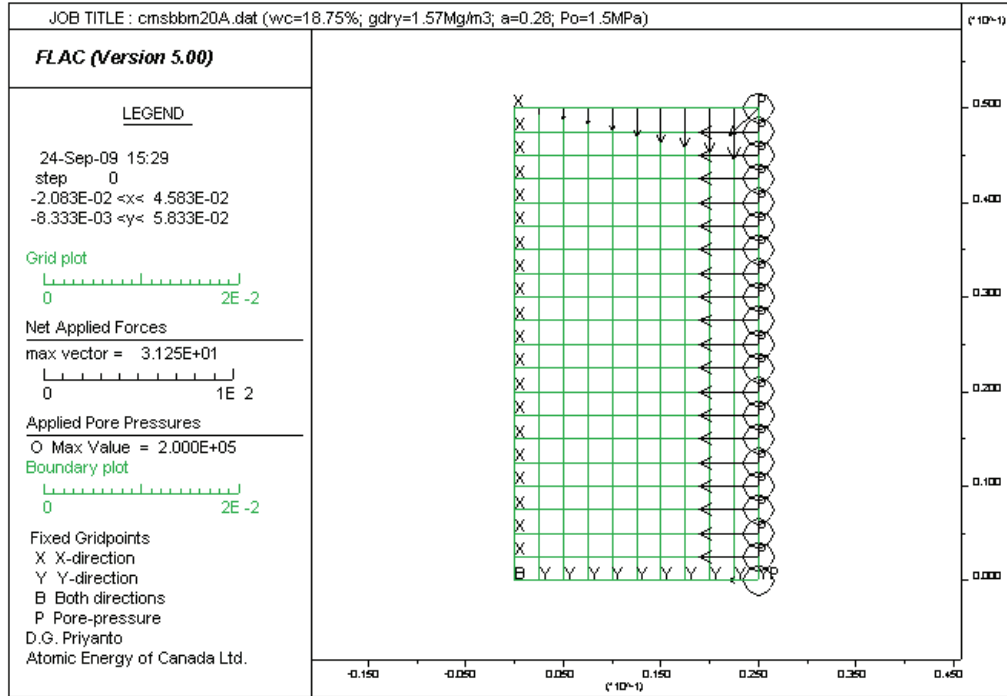
(a) Constant Mean Stress (CMS)
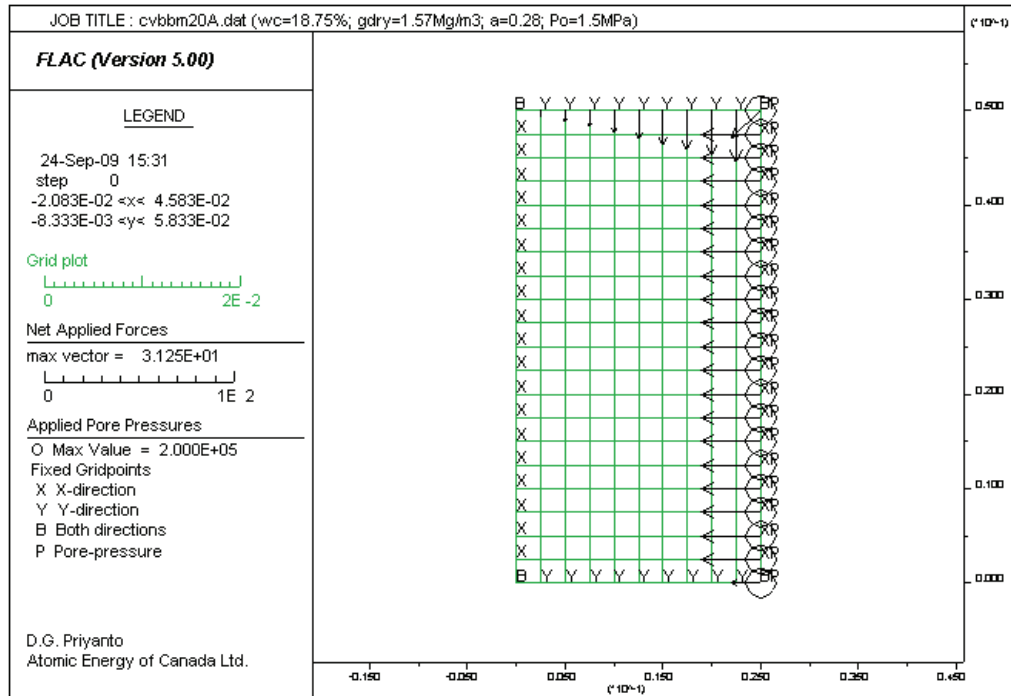
(b) Constant Volume (CV)

Figure 26: Grids and Boundary Conditions used for Analyses using FLAC (10x20 Grids)
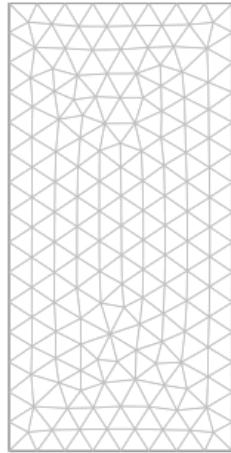
(a) 314 Lagrange-Quadratic Triangular Elements
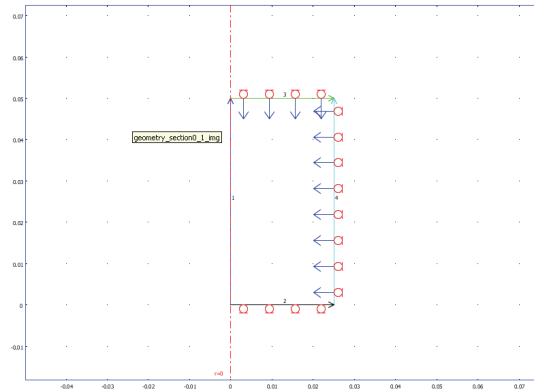
(b) Constant Volume (CV) Boundary Conditions
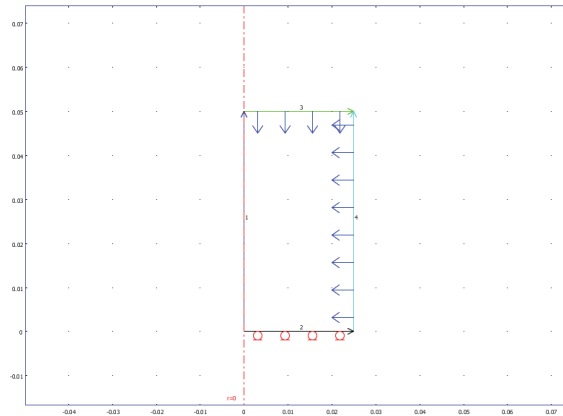
(c) Constant Mean Stress (CMS) Boundary Conditions

Figure 27: Elements used for Analyses using COMSOL (314 Lagrange-Quadratic Triangular Elements)

Table 3: Numerical Modelling of CMS and CV Tests Using Three Different Computer Codes

No.	Type of Triaxial Tests[1]	Computer Code	Analysis Method[2]	Formulations	Mechanical Constitutive Model	Hydraulic Constitutive Model	
						SWCC	Permeability
1.	CMS	CODE_BRIGHT	FEM	One-Phase Flow; Elastoplastic. (constant pore air pressure)	BBM	Van Genuchten	Kozeny's
2.	CMS	FLAC-1	FDM	Two-Phase Flow; Elastoplastic.	BBM-mod[3]	Van Genuchten	Kozeny's
3.	CMS	FLAC-2	FDM	Two-Phase Flow; Elastoplastic.	BSB	Van Genuchten	Kozeny's
4.	CMS	COMSOL	FEM	Richard's Equation, Static	Linear Elastic	Smax Model[4]	Kozeny's
5.	CV	CODE_BRIGHT	FEM	One-Phase Flow; Elastoplastic. (constant pore air pressure)	BBM	Van Genuchten	Kozeny's
6.	CV	FLAC-1	FDM	Two-Phase Flow; Elastoplastic.	BBM-mod[3]	Van Genuchten	Kozeny's
7.	CV	FLAC-2	FDM	Two-Phase Flow; Elastoplastic.	BSB	Van Genuchten	Kozeny's
8.	CV	COMSOL	FEM	Richard's Equation, Static	Linear Elastic	Smax Model[4]	Kozeny's

[1] CV: Constant Volume, CMS: Constant Mean Stress.
[2] FEM: Finite Element Method, FDM: Finite Difference Method.
[3] Modified BBM using Bishop's Effective Stress (Equation 8).
[4] Modified van Genuchten Model with $S_{max} = f(n)$ (Figure 5)

4.4 INPUT DATA

4.4.1 CODE_BRIGHT

Since different computer codes use different notation and assumptions, parameters used for each computer code will be presented separately. Table 4 shows the mechanical parameters

used as input to the CODE_BRIGHT model, while Table 5 shows hydraulic parameters. These parameters in Tables 4 and 5 are similar parameters discussed in Section 3, but they follow the symbols used in the CODE_BRIGHT user's manual. In addition, other parameters (e.g., iteration parameters) required in the analyses are also listed in Tables 4 and 5.

As discussed in Section 3, the critical state slope (M) and stiffness parameter κ change with suction (Figures 11 and 20). Since the CODE_BRIGHT analyses use this original BBM (where M and κ are constant), these characteristics are not included in the original BBM. It is not possible to create a user-defined constitutive model using CODE_BRIGHT and these characteristics cannot be included in the model.

Table 4: Mechanical Data Inputted in CODE_BRIGHT

Mechanical Data		
Thermo Elasto Plastic (TEP): **Elastic Parameters**	**ICL = 21**	$d\varepsilon_v^e = \dfrac{\kappa_i(s)}{1+e}\dfrac{dp'}{p'} + \dfrac{\kappa_s(p',s)}{1+e}\dfrac{ds}{s+0.1} + (\alpha_0)dT$
ITYCL =	1	
P1: κ_{i0}	0.01	where:
P2: κ_{s0}	0.065	
P3: K_{min} (MPa)	0.1	
P5: ν	0.3	$\kappa_i(s) = \kappa_{io}(1+\alpha_i s)$
P8: α_i	-0.003*	$\kappa_s(p',s) = \kappa_{s0}(1+\alpha_{sp}\ln(p'/p_{ref}))$
P9: α_{sp}	-0.147*	
P10: p_{ref} (MPa)	0.01	
Thermo Elasto Plastic (TEP): **Plastic Parameters (1)**	**ICL = 23**	$p_0 = p^c\left(\dfrac{p_0^*(T)}{p^c}\right)^{\frac{\lambda(0)-k_{io}}{\lambda(s)-k_{io}}}$
ITYCL =	1	
P1: $\lambda(0)$	0.26	
P2: r	0.22	$\lambda(s) = \lambda(0)[(1-r)\exp(-\beta s)+r]$
P3: β (MPa^{-1})	0.30	$p_s = p_{s0} + ks\exp(-\rho\Delta T)$
P4: ρ (°C^{-1})	0.2*	
P5: k	0.021	
P6: p_{s0} (MPa)	0.1	
Thermo Elasto Plastic (TEP): **Plastic Parameters (2)**	**ICL = 24**	
ITYCL =	1	
P1: p^c (MPa)	0.34	
P2: M	1.0	
P3: α	0.3*	
P4: e_0	0.6	
P5: p_0* (MPa)	0.5	
Thermo Elasto Plastic (TEP): **Parameter shape yield surface**	**ICL = 25**	$G_y(\theta) = 1$
ITYCL =	3*	Von Mises (default option)
Thermo Elasto Plastic (TEP): **Parameter shape plastic potential**	**ICL = 26**	$G_p(\theta) = 1$
ITYCL =	3*	Von Mises (default option)
Thermo Elasto Plastic (TEP): **Parameter shape plastic potential**	**ICL = 27**	
ITYCL =	1	
P1: Tole1	1.e-8	
P2: Tole2	1.e-3	
P3: Tole3	1.e-3	
P4: μ	1	
P5: Index	-1	Elastoplastic Matrix

Default values from CODE_BRIGHT examples are used.

Table 5: Hydraulic Data

Hydraulic Data		
Retention Curve	ICL = 6	Van Genuchten Model
ITYCL :	1	$$S_e = \frac{S_l - S_{rl}}{S_{ls} - S_{rl}} = \left(1 + \left(\frac{P_g - P_l}{P}\right)^{\frac{1}{1-\lambda}}\right)^{-\lambda}$$ $$P = P_0 \frac{\sigma}{\sigma_0}$$
P1: P_0 (MPa)	1.512	
P2: σ_0 (N m^{-1})	0.072	
P3: λ	0.28	
P4: S_{rl}	0.0	
P5: S_{ls}	1	
Intrinsic Permeability	ICL = 7	Darcy's Law:
ITCLY	1	$$\mathbf{q}_l = -\frac{\mathbf{k} k_{rl}}{\mu_l}(\nabla P_l - \rho_l \mathbf{g})$$
P1: $(k_{11})_0 (m^2)$	1.e-19	Kozeny's model:
P2: $(k_{22})_0 (m^2)$	1.e-19	$$\mathbf{k} = \mathbf{k_0} \frac{\phi^3}{(1-\phi)^2}\frac{(1-\phi_0)^2}{\phi_0^{\;3}}$$
P3: $(k_{33})_0 (m^2)$	1.e-19	
P4: ϕ_0	0.42	
P5: ϕ_{min}	0.001	
Liquid Phase Relative Permeability	ICL =14	Van Genuchten model: $$k_{rl} = \sqrt{S_e}\left(1 - \left(1 - S_e^{1/\lambda}\right)^\lambda\right)^2$$
ITCLY	1	
P3: λ	0.28	
P4: S_{rl}	0.0	
P5: S_{ls}	1.0	
Diffusive flux of vapour:*	ICL = 11	Fick's law for molecular diffusion:
ITYCL	1	$$\mathbf{i}_g^w = -\left(\tau\phi\rho_g S_g D_m^w \mathbf{I}\right)\nabla \varpi_g^w$$
P1: D (m^{2}s^{-1} K^{-n} Pa)	5.9e-6*	$$D_m^{vapour} = D\left(\frac{(273.15 + T)^n}{P_g}\right)$$
P2: n	2.3*	
P3: τ_0	0.8	τ = constant = τ_0
Phase Properties		
Solid Phase	ICL=10	
ITYCL	1	
P2: ρ_s (kg m^{-3})	2700	

* Default values from CODE_BRIGHT examples are used.
  **ICL and ITYCL are the notations used to input the data in the CODE_BRIGHT

4.4.2 Modelling Using FLAC

FLAC with two-phase flow options was used to simulate the HM behaviour of the BSB. A user-defined constitutive model can be created in FLAC and more features of the BSB specimens in section 3 can be included in the simulation.

Two models were used in the analyses using FLAC, including:
1. the BBM-mod; and
2. the BSB model.

1. The BBM-mod

The BBM-mod is the modification of the original BBM using different stress state variable. Unlike the original BBM (Alonso et al. 1990) that uses net mean stress (Equation 7), the BBM-mod uses Bishop's effective stress (Equation 8). The mechanical parameters used to simulate the BSB materials using the BBM-mod are listed in Table 2. In addition of these mechanical parameters, the hydraulic parameters are used in FLAC analyses, including: the van Genuchten's SWCC during wetting in Table 1 and Kozeny's model in Section 3.1.3.

2. The BSB model

During the calibration process, the coupling of the LC-line (Figure 1b) and coefficient of compressibility (λ) in the BBM limited the ability to match the model response with laboratory test results. In order to remove this limitation the yield line and coefficient of compressibility are uncoupled in the new model, called the BSB model.

In the BSB model, the critical state slope (M) and the coefficient of compressibility (κ) are a function of suction. Previously in Section 3, the relationship of M and s can be defined by Equations 26a-26c, which is a discontinuous function. It is beneficial to have continuous functions in the implementation of a constitutive model in a computer code. SWCC of van Genuchten model is a continuous function. The BSB model couples the parameters M, κ, and λ with the SWCC. Since suction (s) is a function of effective saturation (S_e) in the SWCC, parameters κ, λ, M, and p_0 are defined as a function of S_e. The equations used for the BSB Model are listed as follows.

- The dependence of coefficient of compressibility (κ) with effective saturation (S_e):

$$\kappa(s) = \kappa_{min} + S_e \cdot \left(\kappa_{max} - \kappa_{min}\right) \qquad (27)$$

- The dependence of coefficient of compressibility (λ) with effective saturation (S_e):

$$\lambda(s) = \lambda_{max} - S_e \cdot \left(\lambda_{max} - \lambda_{min}\right) \qquad (28)$$

- The dependence of critical state slope (M) with effective saturation (S_e):

$$M(s) = M_{min} + S_e \cdot \left(M_{max} - M_{min}\right) \qquad (29)$$

- The yield line $p_0(s)$ with suction (s):

$$p_0(s) = (p^*_0 + r \cdot s) + S_e \cdot s \qquad (30)$$

where:
- S_e is the effective saturation calculated from the SWCC in Equations (1) to (3).
- Parameters κ_{min} and κ_{max} are minimum and maximum coefficients of compressibility observed from isotropic loading-unloading test (Figure 11).
- Parameters λ_{min} and λ_{max} are the minimum and maximum coefficients of compressibility observed from isotropic loading-unloading test (Figure 12).

- Parameters M_{min} and M_{max} are the minimum and maximum critical state slopes (Figure 20).
- p_0^* is the preconsolidation pressure at saturated conditions.
- r is a fitting parameter
- S_e and s is the effective degree of saturation and suction from SWCC relationship (Equations 1 to 3)

The BSB model parameters used to simulate the BSB are listed in Table 6. In addition of these mechanical parameters, the hydraulic parameters are used in the BSB model, including: the van Genuchten's SWCC during wetting in Table 1 and Kozeny's model in Section 3.1.3.

Table 6: Parameter Used for the BSB Model

Parameters	Value
κ_{min}	0.005
κ_{max}	0.01
λ_{min}	0.13
λ_{min}	0.025
M_{min}	0.5
M_{max}	1.2
p_0^* [MPa]	0. 5
r	0.05

4.4.3 Modelling Using COMSOL

The laboratory test results of BSB specimens show the dependent of the maximum degree of saturation (S_{max}) as a function of porosity (n) (Figure 5, Section 3.1.2), which is called Smax model in this document. Implementation of the Smax model requires modification of the governing equations, which was not possible using either CODE_BRIGHT or FLAC. Alternatively, COMSOL allows the user to modify the governing equation to implement this feature.

COMSOL is a finite element computer code for multi-physics numerical modelling. Not all features for THM analysis of unsaturated soil have been included in the code by the developer, but the user can add additional formulations/ processes and coupling as required. The following custom-additions in COMSOL have been generated in this study, including:
- Coupling of Richard's equation and linear elastic model to simulate H-M processes under unsaturated condition; and
- Implementation of Smax model, which has SWCC and permeability functions with S_{max} as a function of total porosity.

4.4.3.1 Governing Equations and Parameters

The governing equations used in the analysis are as follows.
Unsaturated flow is described using Richard's equation:

$$\left[C + S_e S \right] \frac{\partial H_p}{\partial t} + \nabla \cdot \left[-K \nabla \left(H_p + D \right) \right] = Q_s \tag{31}$$

Pressure head, H_p [m] is the output of the hydraulic analysis using COMSOL and pore pressure, $p = H_p/(g \cdot \rho_f)$. Using this equation pore air pressure is assumed as constant and equal to 0 so that suction ($s = -p$) and hence $H_p = -s \cdot g \cdot \rho_f$. C denotes specific moisture capacity [m^{-1}], S_e is the effective saturation, S is the storage coefficient (m^{-1}), t is the time, K is the hydraulic conductivity (m/s), and D is the vertical elevation, and ρ_f is the fluid density

In Equation 31, the first term represents the change in storage in the unsaturated material, while the second term represents Darcy's law with a hydraulic conductivity that is dependent upon saturation. S is the specific storage, which is set as follows.

$$S = \rho_f g \left(\chi_p + \theta \chi_f \right) \tag{32}$$

where:

ρ_f is the fluid density,
g is the acceleration of gravity,
χ_p and χ_f are the compressibilities of the solid particles and fluid, respectively.

The hydraulic conductivity, K is:

$$K = k_w^{sat} \cdot k_r \tag{33}$$

k_w^{sat} is the hydraulic conductivity at saturated conditions [m/s] and dependent on the total porosity. Kozeny's equation (Equation 6) is used to define this relationship. k_r is the relative permeability described using van Genuchten (1980) equations.

$$k_r = \begin{cases} S_e^{L} \left[1 - \left(1 - S_e^{1/m} \right)^m \right]^2 & \text{for } H_p < 0 \\ 1 & \text{for } H_p \geq 0 \end{cases} \tag{34}$$

S_e and C are also calculated using van Genuchten (1980) equations.

$$S_e = \begin{cases} \dfrac{1}{\left[1 + \left| \alpha H_p \right|^n \right]^m} & \text{for } H_p < 0 \\ 1 & \text{for } H_p \geq 0 \end{cases} \tag{35}$$

$$C = \begin{cases} \dfrac{\alpha m}{1 - m} \left(\theta_s - \theta_r \right) S_e^{\frac{1}{m}} \left(1 - S_e^{\frac{1}{m}} \right)^m & \text{for } H_p < 0 \\ 0 & \text{for } H_p \geq 0 \end{cases} \tag{36}$$

α, m, n, and L are fitting parameters. θ_s and θ_r are the saturated and residual volumetric water content.

In this analysis saturated volumetric water content (θ_s) is equal to the current total porosity (θ) that is calculated using:

$$\theta = (v - 1)/v \tag{37}$$

v is the total specific volume, calculated from:

$$v = v_{initial} \cdot (1+\varepsilon_v) \tag{38}$$

$v_{initial}$ (=1/(1-$\theta_{initial}$)) is the initial specific volume. ε_v is the volume strain.

The mechanical to hydraulic (MH) coupling is done by substitution of the flow (Q_s) in Equation 31 with the following equations:

$$Q_s = -\alpha_b \cdot \frac{\partial}{\partial t}(\nabla \cdot u) \tag{39}$$

$\frac{\partial}{\partial t}(\nabla \cdot u)$ is the time rate change of strain, u is the displacement vector and α_b is a constant usually termed as Biot-Willis coefficient.

The hydraulic to mechanical (HM) coupling is done by application of the body force induced by the hydraulic process.

$$\mathbf{F} = -\alpha_b\, \rho_f\, g\, \nabla H \tag{40}$$

In this analysis a linear elastic model is used.

4.4.3.2 Calculation of Residual Porosity (θ_r)

The implementation of Smax model in COMSOL is completed by as follows. Figure 5 in Section 3.1.2 shows that the maximum degree of saturation (S_{max}) of the BSB specimens increases with total porosity. With known value of S_{max}, the residual volumetric water content is equal to:

$$\theta_r = (1-S_{max}) \cdot \theta \tag{41}$$

The current degree of saturation (S_w) is equal to:

$$S_w = S_e\, (\theta - \theta_r)/\, \theta \tag{42}$$

These formulations have been added in the analyses using COMSOL and the parameters used in the analyses listed in Table 7.

Table 7: Parameters used in COMSOL Analysis

Variables	Units	Descriptions	Value
g	m/s^2	Gravity	9.82
ρ_f	kg/m^3	Fluid density	1000
χ_p	m·s^2/kg	Compressibility of solid particles	10^{-8}
χ_f	m·s^2/kg	Compressibility of fluid particles	4.4·10^{-10}
α	m^{-1}	Alpha parameter	0.00327
n		N parameter	1.39
m		1-1/n	0.28
L		L parameter	0.5
$\theta_{initial}$		Initial porosity	0.42
k_{sat}	m/s	Kozeny's Equation (Substitution of $k_0 = 5 \cdot 10$ m/s, $n_0 = 0.42$ in Equation 6)	Function of θ

5. RESULTS AND DISCUSSION

5.1 COMPARISON OF DIFFERENT ANALYSES

Eight analyses have been completed to simulate constant volume (CV) and constant mean stress (CMS) tests using three different computer codes (CODE_BRIGHT, FLAC, and COMSOL) with the configuration shown in Table 3. The objectives of this discussion are to compare analyses using different computer codes and evaluate the effects on the results of different features in the constitutive models and formulations used in the analyses.

The volume of water added to the specimen was calculated for each analysis and compared to the results of laboratory tests with CV and CMS conditions as shown in Figures 28. In the CV test, the volume of water added to the specimen analyzed using COMSOL matched the laboratory test results well after 5 days. FLAC-BBM-mod and FLAC-BSB analyses, as well as CODE_BRIGHT analysis overestimated the laboratory test results (Figure 28a). For CMS tests, FLAC-BBM-mod and FLAC-BSB analyses matched the laboratory test results well (Figure 28b). COMSOL model underestimated the laboratory test results, while CODE_BRIGHT analysis overestimated the laboratory test results.

The COMSOL analyses used the Smax model having S_{max} in the SWCC as a function of total porosity (Figure 5). The Smax model prevented the results of the numerical model to reach 100% saturation, similar to what was observed in the laboratory test results. Compared to the other models, COMSOL analyses using the Smax model can give a reasonable prediction of the volume of water added to the specimen in the CV test (Figure 28a). As expected due to the limitation of the linear elastic (LE) model, the CMS test did not provide a good match to the volume added (Figure 28b). In the CV test, the total volume was always constant and the mechanical constitutive model did not have significant effect in the prediction of total volume of water added to the specimen. The total volume changes during the CMS test the mechanical

constitutive model had more effect in the prediction of total volume of water added to the specimen.

Figure 28 shows the difference between FLAC-BBM-mod and CODE_BRIGHT analyses in CV and CMS tests. The parameters were similar for both analyses. These differences were likely due to the following two reasons. First, FLAC-BBM-mod used the Bishop's effective stress (Equation 8), while CODE_BRIGHT used net mean stress (Equation 7). Second, FLAC-BBM-mod used two-phase flow, while CODE_BRIGHT used one-phase flow formulations.

Both COMSOL and CODE_BRIGHT used the Finite Element Method (FEM), while FLAC-BBM-mod and FLAC-BSB used the Finite Difference Method (FDM). Both COMSOL and CODE_BRIGHT analyses used one-phase flow formulation with an assumption of constant pore air pressure (u_a), while FLAC used two-phase flow formulation. The difference between these analyses (FEM with one-phase flow versus FDM with two phase flow) can be observed in Figure 28a and 28b. Since different numerical modelling methods (FEM versus FDM) should not have significant effects on the results, the difference between these models was more likely due to one- or two- phase flow formulations. The results using two-phase flow show smooth transition to reach equilibrium (FLAC-BBM-mod and FLAC-BSB in Figures 28a and 28b), in contrast clear transition before and after equilibrium are shown in the results of the analysis using one-phase flow (CODE_BRIGHT and COMSOL in Figures 28a and 28b). Achieving equilibrium is indicated by achieving a no further change in the volume of water added to the specimen and constant suction.

The average suctions from four analyses were compared to the laboratory test results (Figure 29). Smooth transitions of suction were observed when using two-phase flow and suctions at the end of test were greater than zero, as it was also observed in the laboratory test (FLAC-BBM and FLAC-BSB in Figure 29). Analyses using one-phase flow did not show smooth transition and the suction at the end of test were equilibrated to the applied pore water pressure of 0.2 MPa (i.e., suction ~ -0.2 MPa).

The changes of volume strain during CMS test are shown in Figure 30. Analyses using CODE_BRIGHT and COMSOL matched the laboratory test results, while FLAC underestimated the laboratory test results. This could be due to the different stress-state variables (e.g., Bishop's effective stress versus net mean stress) used in the analyses.

The average total mean stress during constant volume tests is shown in Figure 31. FLAC-BBM-mod and FLAC-BSB analyses matched the laboratory test results, while CODE_BRIGHT analysis underestimated the laboratory test results. These three analyses used an elasto-plastic constitutive model. COMSOL, which used a linear elastic constitutive model, overestimated the average total mean stress. This figure shows the significance using elasto-plastic models to estimate total mean stress.

FLAC-BSB removed the coupling of yield line and coefficient of compressibility in the FLAC-BBM-mod. Comparison of total mean stress from FLAC-BBM-mod and FLAC-BSB (Figure 31) shows that slight improvement of the matching of total mean stress when using the BSB model.

The main difference between FLAC-BBM-mod and FLAC-BSB are the variations of coefficient of compressibility κ and critical state slope M with effective saturation (S_e). The FLAC-BBM-mod used constant κ and constant M, while the FLAC-BSB used κ and M as a function of S_e. Since S_e is a function of s, as defined by SWCC, there was no significant difference between

the results of two analyses for limited suction changes (e.g., 0-3 MPa). However, that may not be the case when the range of suction changes are substantial (in the range of 0 to >100 MPa), such as discussed in Section 3.

Gravimetric water content, degree of saturation, and dry density at the end of test were compared to the laboratory CV and CMS tests results, respectively (Figures 32 and 33). The analyses using CODE_BRIGHT overestimated the magnitude of the gravimetric water content at the end of laboratory CV (Figure 32a) and CMS tests (Figure 33a). The analyses using FLAC-BSB and FLAC-BBM-mod provided a reasonable match with end of test data for the CMS test (Figure 32a), but not for the CV test (Figure 33a). The analyses using COMSOL matched the magnitude of the gravimetric water content at the end of laboratory CV and CMS tests, but they did not predict the trend of laboratory test data. The laboratory test data showed an increase of water content with increasing radial distance, while COMSOL analyses resulted in uniform gravimetric water content with radial distance (Figures 32a and 33a). This is expected due to the linear elastic model used in COMSOL.

The results of CV and CMS tests in the laboratory show variation of the dry density and degree of saturation with the radial distance (Figures 32b-c and Figures 33b-c). This variation can be simulated using the elasto-plastic model, but not the linear elastic model. Using elasto-plastic model in the analyses (CODE_BRIGHT, FLAC-BBM-mod, FLAC-BSB), resulted in slight variation of dry density at the end of test (Figures 32bc and 33b-c). Using linear elastic model (COMSOL), the degree of saturation and dry density at the end of test were uniform with radial distance (Figures 32b-c and 33b-c).

The degree of saturation observed at the end of CV and CMS tests in the laboratory was less than 100% (Figures 32b and 33b). In order to match these results, S_{max} as a function of total porosity should be included in the model. This feature was included in the COMSOL analyses, but not in the other analyses (FLAC-BBM-mod, FLAC-BSB and CODE_BRIGHT). Figures 32b and 33b show that the magnitude of the degree of saturation of the COMSOL analyses was closer to the laboratory test results and less than the other analyses.

Due to boundary conditions applied in the CV test, the average dry density was constant throughout the test. The computed dry density at the end of the CV test indicated only a slight difference between each model (Figure 32c). For the CMS tests (Figure 33c), the magnitude of CODE_BRIGHT model was the closest to the laboratory data, but the trend of the dry density with radial distance was the opposite of the laboratory test results. Other models overestimated the magnitude of dry density at the end of laboratory test.

Hydraulic and mechanical behaviours of the BSB are related to each other. In order to match both magnitude and trend of the laboratory test data all the features of the BSB in section 3 simultaneously. Since none of the models presented in this document have included all these features simultaneously, it should be expected that none of the models provided good matches in both magnitude and trend with measured end of test saturation or dry density.
CODE_BRIGHT and FLAC used elastoplastic model, but not the Smax model. COMSOL used the Smax model, but not the elastoplastic model. It is recommended to incorporate all the BSB model and Smax model simultaneously in order to provide good matches with the laboratory test measurements.
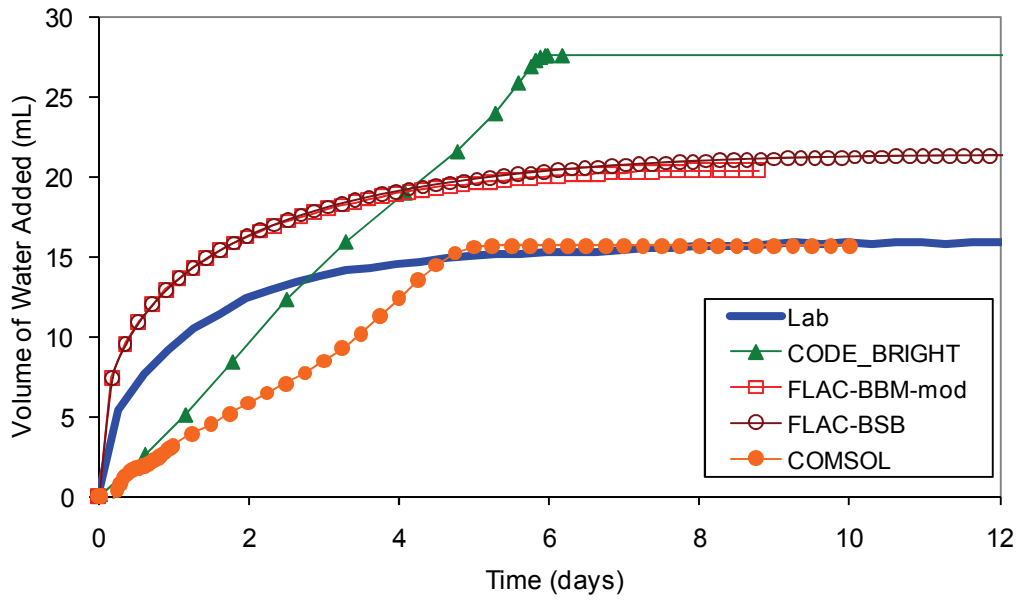
(a) Constant Volume (CV) Test
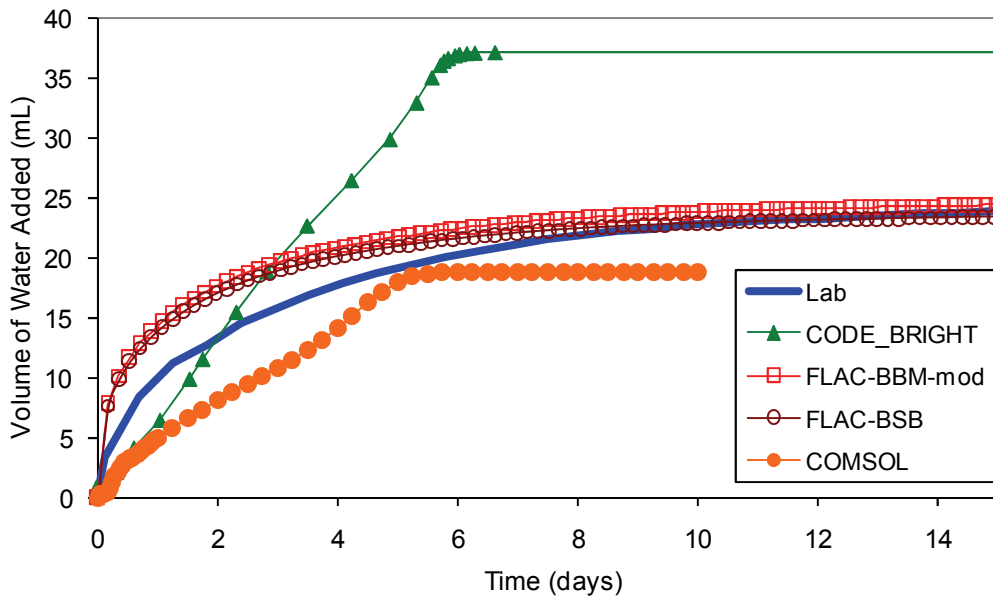
(b) Constant Mean Stress (CMS) Test

Figure 28: Volume of Water Added to The Specimen
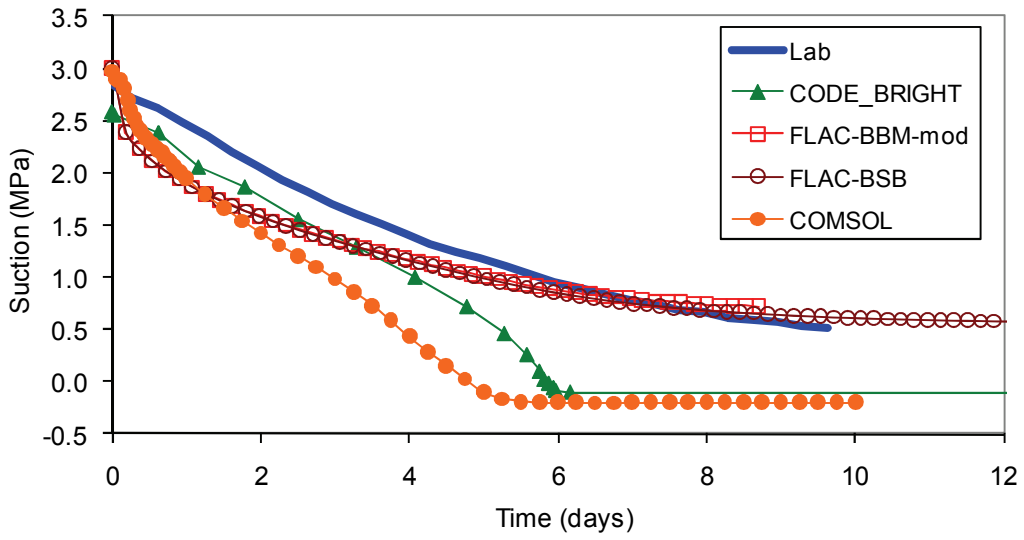
(a) Constant Volume (CV) Test
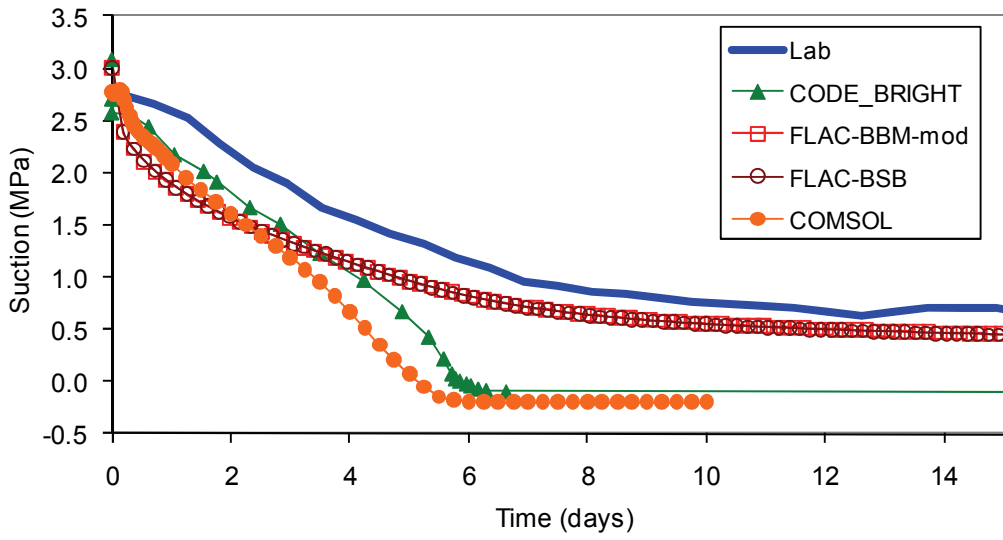
(b) Constant Mean Stress (CMS) Test

Figure 29: Average Suction of the Specimen
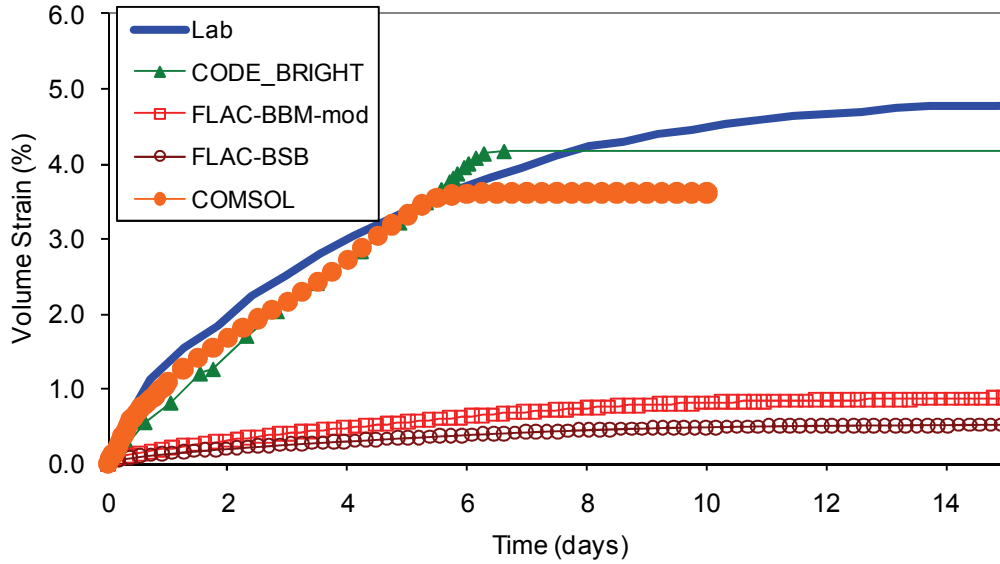
Figure 30: Volume Strain of the Constant Mean Stress (CMS) Test
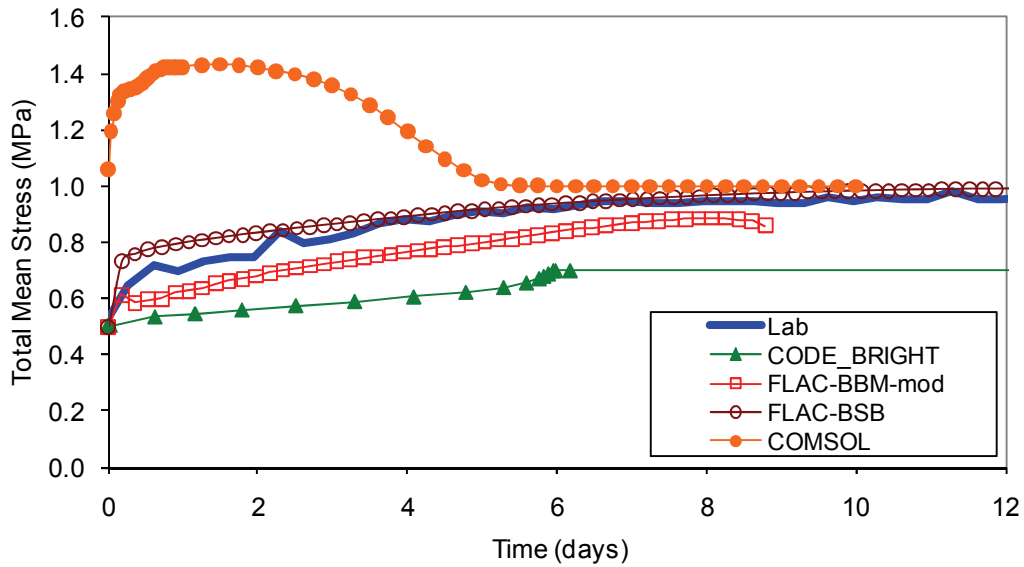
Figure 31: Average Total Mean Stress of the Constant Volume (CV) Test
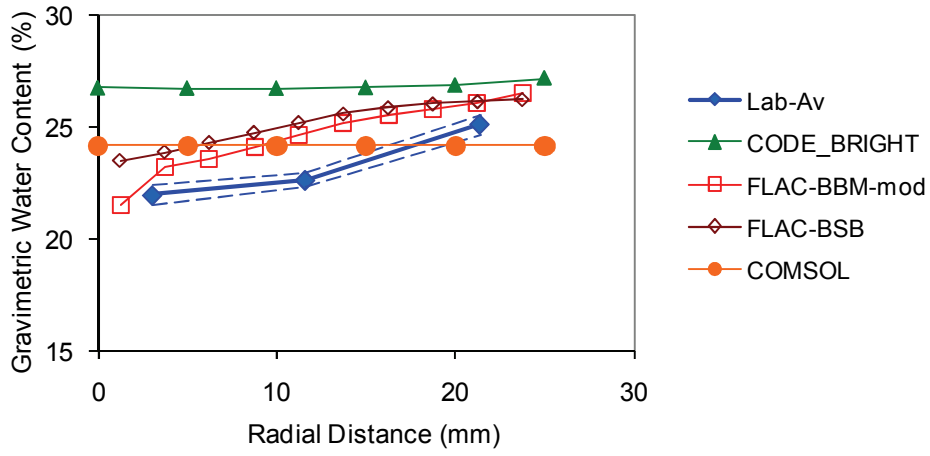
(a) Gravimetric Water Content
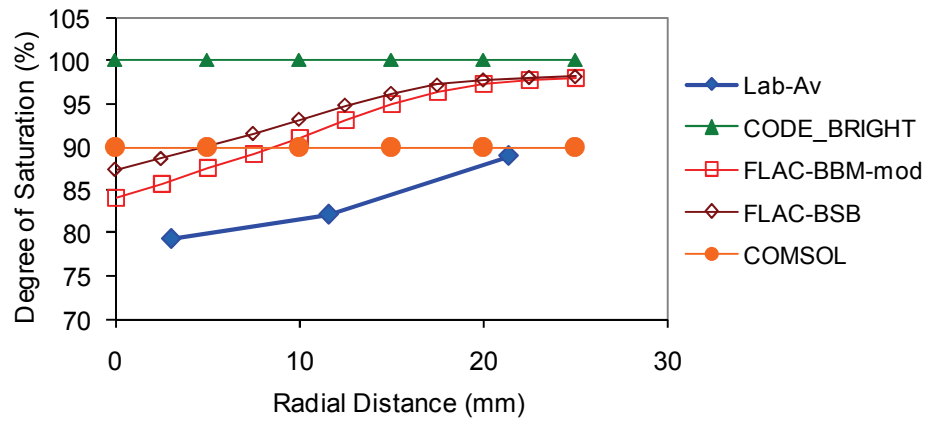
(b) Degree of Saturation
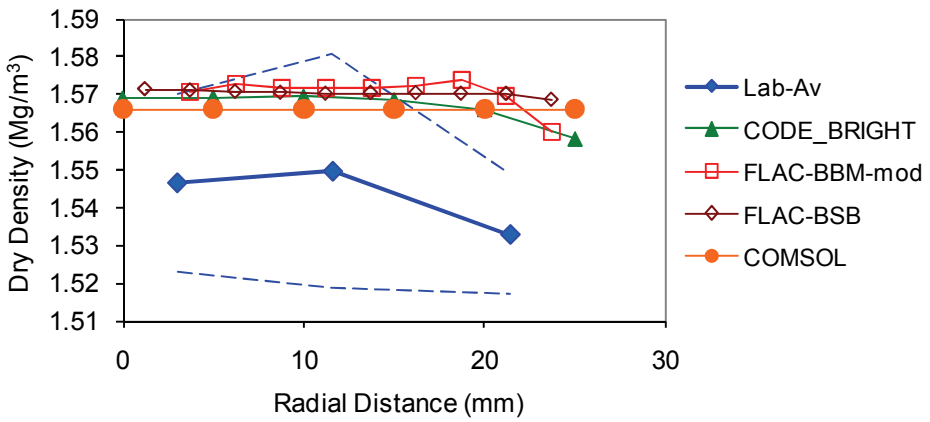
(c) Dry Density

Figure 32: The End of Test Properties after Constant Volume (CV) Tests
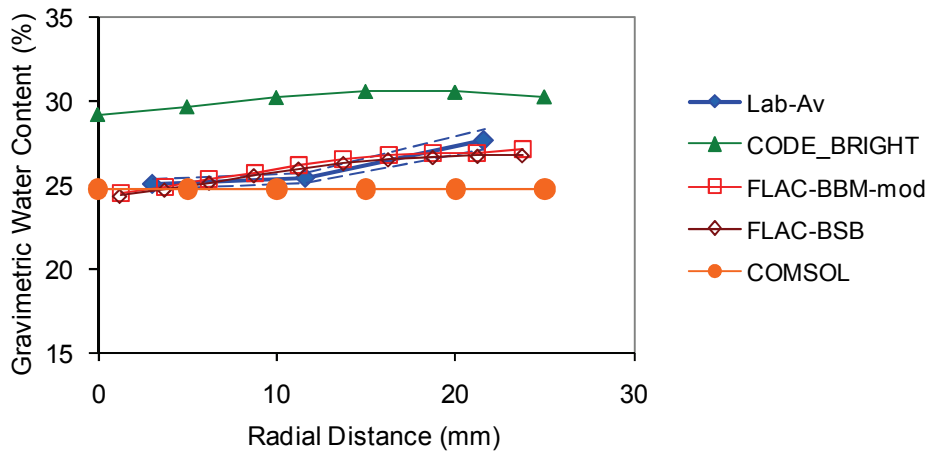
(a) Gravimetric Water Content
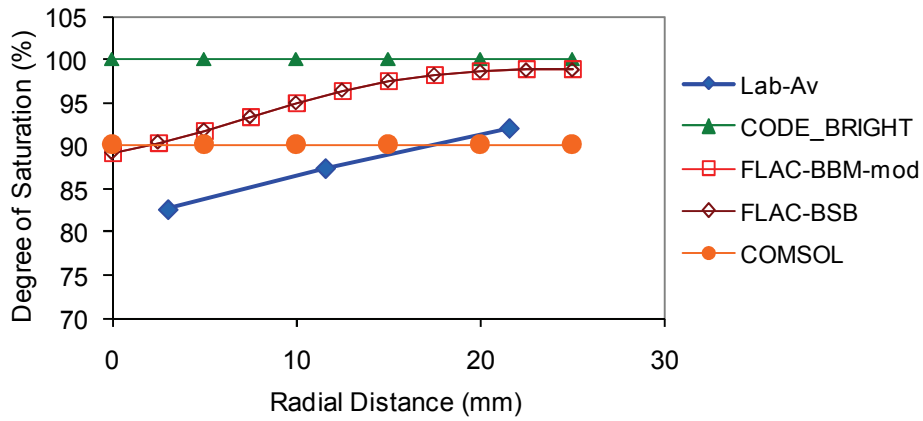
(b) Degree of Saturation
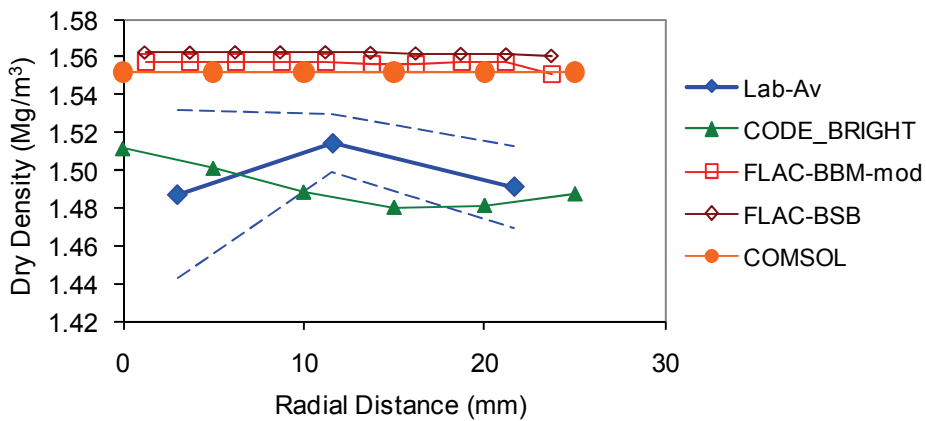
(c) Dry Density

Figure 33: The End of Test Properties after Constant Mean Stress Tests

5.2   EVOLUTION OF DEGREE OF SATURATION AND DRY DENSITY

In this discussion the mid-layer is located at the symmetry line in Figure 24. Figures 34 and 35 show the evolution of the degree of saturation at the mid-layer of the analyses using CODE_BRIGHT, FLAC-BSB, and COMSOL for CV and CMS tests, respectively. The changes of degree of saturation contours during CV tests for analyses using CODE_BRIGHT, FLAC-BSB, and COMSOL are shown in Figures 36, 37, 38, respectively. All of the analyses show an increase of degree of saturation starting with the outside perimeter (x = 25 mm) of the specimen followed by the layer close to the centre (x < 25 m) (see Figure 24 for the location of x-axis). At the end of test in CODE_BRIGHT analyses, the degree of saturation reached 100% saturation (Figure 34a and 35a). FLAC-BSB analyses reached almost 100% saturation (Figures 34b and 35b). The maximum degree of saturation in the COMSOL analysis was set as a function of porosity using the Smax model. The porosity was inversely proportional to a dry density. The degree of saturation at the end of test was equal to ~ 90% corresponding to a dry density of 1550 to 1565 kg/m^3 (shown in Figures 34c, 35c and 39).

The degree of saturation contours from all the analyses (Figures 36, 37, 38) show a similar trend, but different magnitudes. The water flow was mainly radial flow where axial variations of the degree of saturation were not noticeable.

Evolution of the dry density in the mid-layer of the specimen from the results of the analyses using CODE_BRIGHT, FLAC-BSB, and COMSOL for CV and CMS tests are shown in Figures 39 and 40. Variation of the dry density at the equilibrium state analysed using elasto-plastic model were noticeable (i.e., CODE_BRIGHT (Figures 39a and 40a) and FLAC-BSB (Figures 39b and 40b)), as they were in the laboratory test results. When using the linear elastic model (e.g., in COMSOL), there was no variation of dry density at the end of tests (Figures 39c and 40c). This comparison shows the significance of using an elasto-plastic model to simulate clay-based sealing material behaviour. In this particular case, the application of the elastoplastic model can improve the matching of laboratory test results in trend, but not in the magnitude.
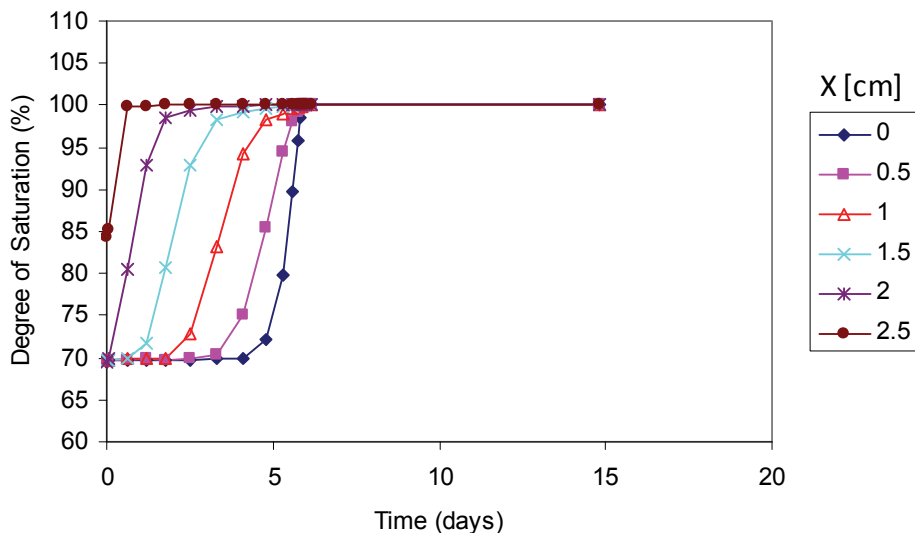
(a) CODE_BRIGHT
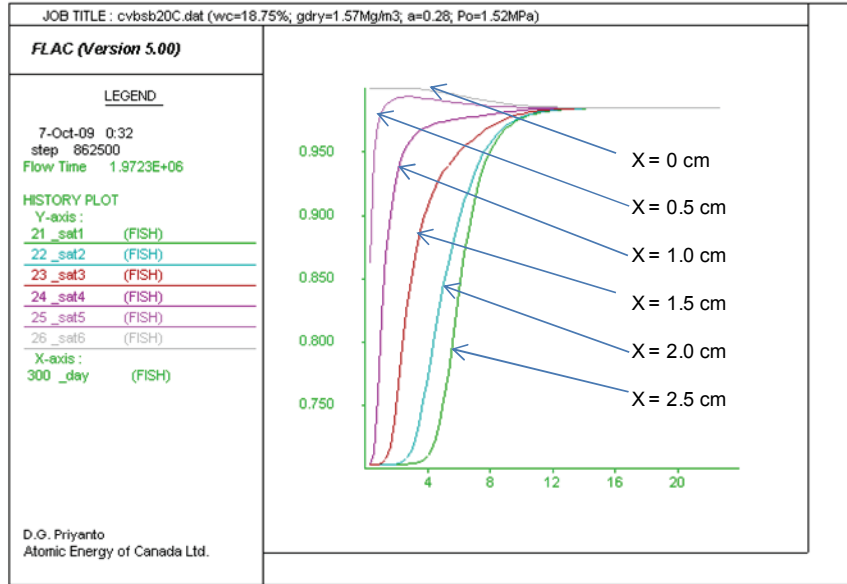
(b) FLAC-BSB Model
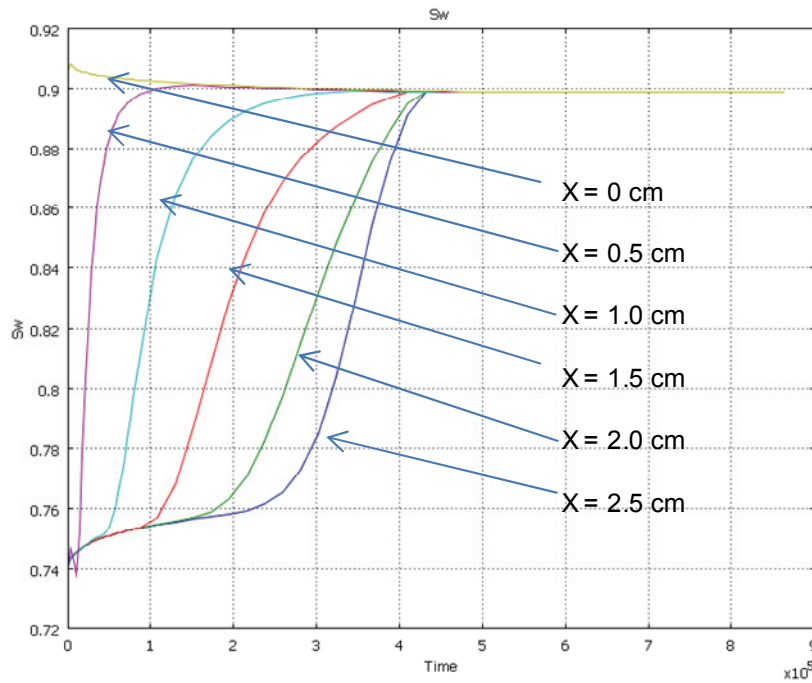
(c) COMSOL

Figure 34: Evolution of Degree of Saturation (CV) (X is the radial distance refer to Figure 24a)
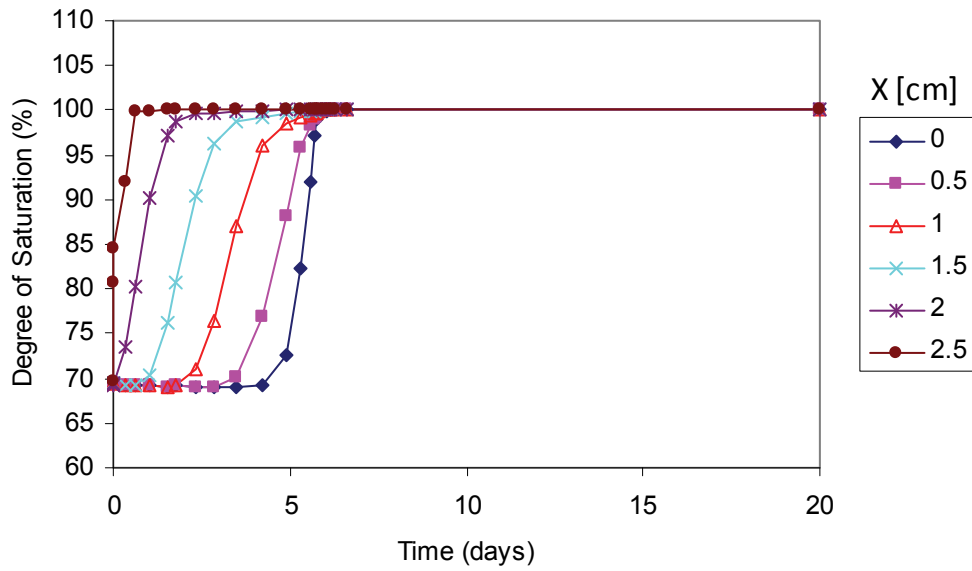
(a) CODE_BRIGHT
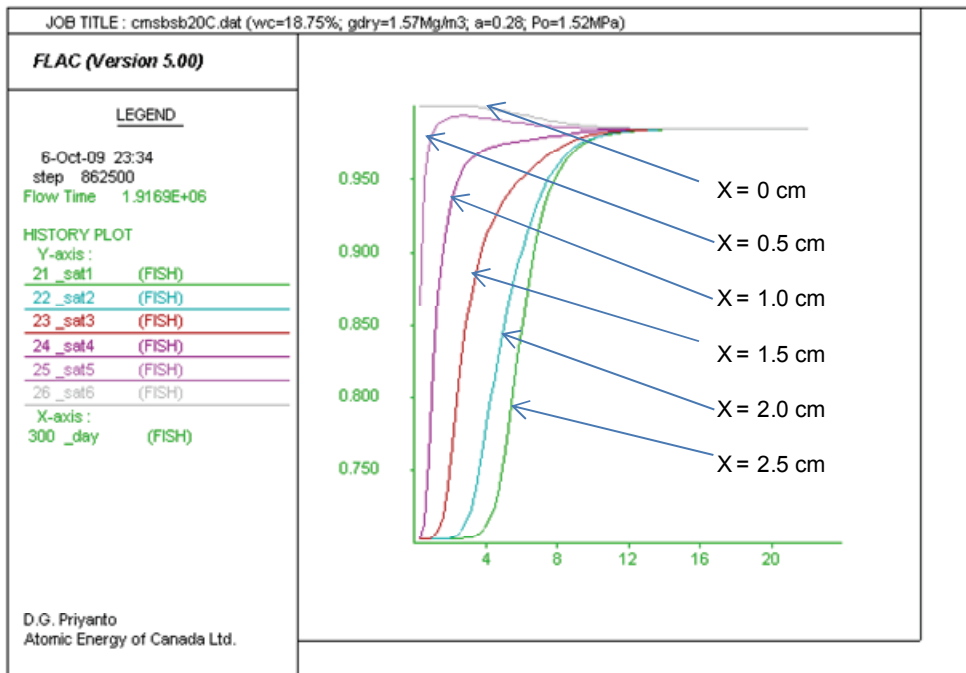
(b) FLAC-BSB Model

(c) COMSOL
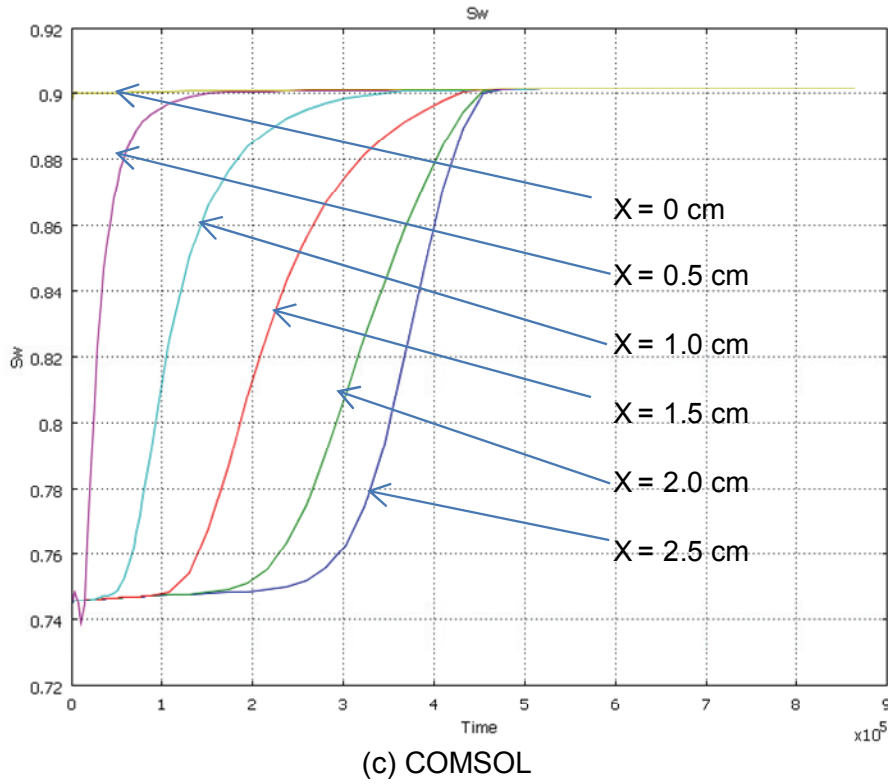
Figure 35: Evolution of Degree of Saturation (CMS) (x is the radial distance refer to Figure 24a)

~1.05 days   2.3 days   4.2 days   6.62 days   20 days
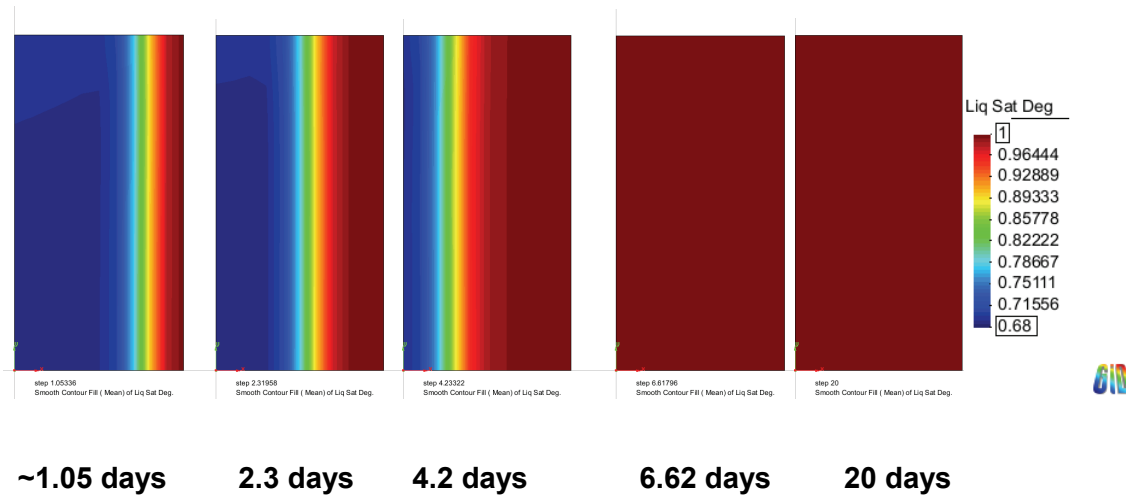
Figure 36: Degree of Saturation Contour from CODE_BRIGHT Model of Constant Mean Stress (CMS) Test at Different Times

Saturation contours	Saturation contours	Saturation contours	Saturation contours
7.00E-01	7.00E-01	8.50E-01	9.85E-01
7.50E-01	7.50E-01	8.75E-01	9.85E-01
8.00E-01	8.00E-01	9.00E-01	9.85E-01
8.50E-01	8.50E-01	9.25E-01	9.85E-01
9.00E-01	9.00E-01	9.50E-01	9.85E-01
9.50E-01	9.50E-01	9.75E-01	9.85E-01
			9.85E-01
			9.85E-01
~ 3.65 hours	~ 1.06 days	~ 6.04 days	~ 14.9 days
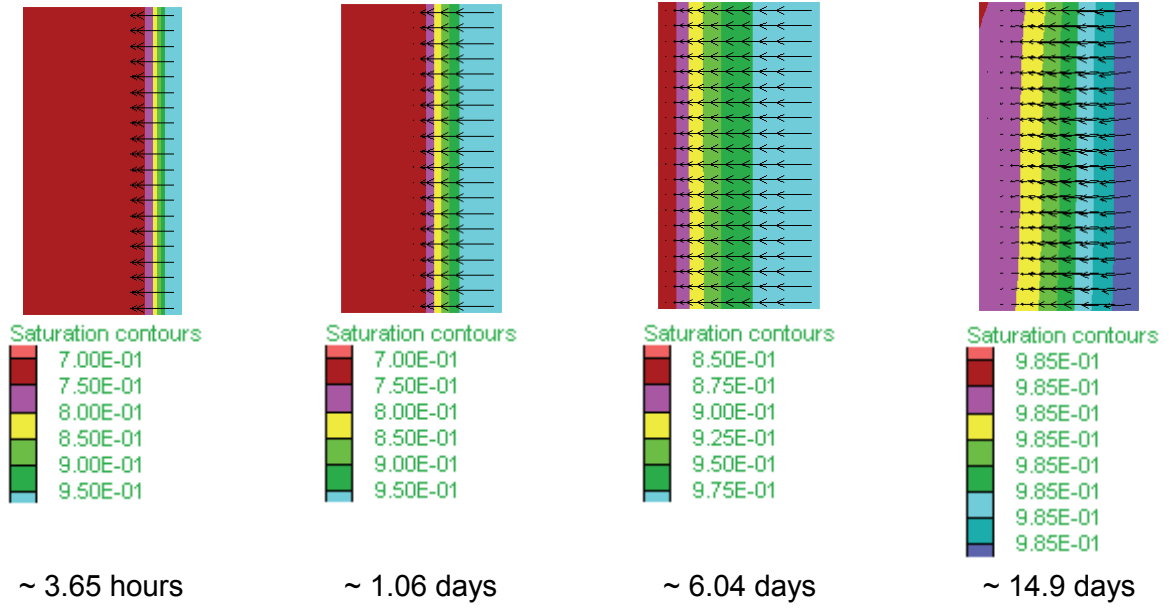
Figure 37: Degree of Saturation Contour from FLAC-BSB Model of Constant Mean Stress (CMS) Test at Different Times

(1 hour)   (1 day)   (6.25 days)
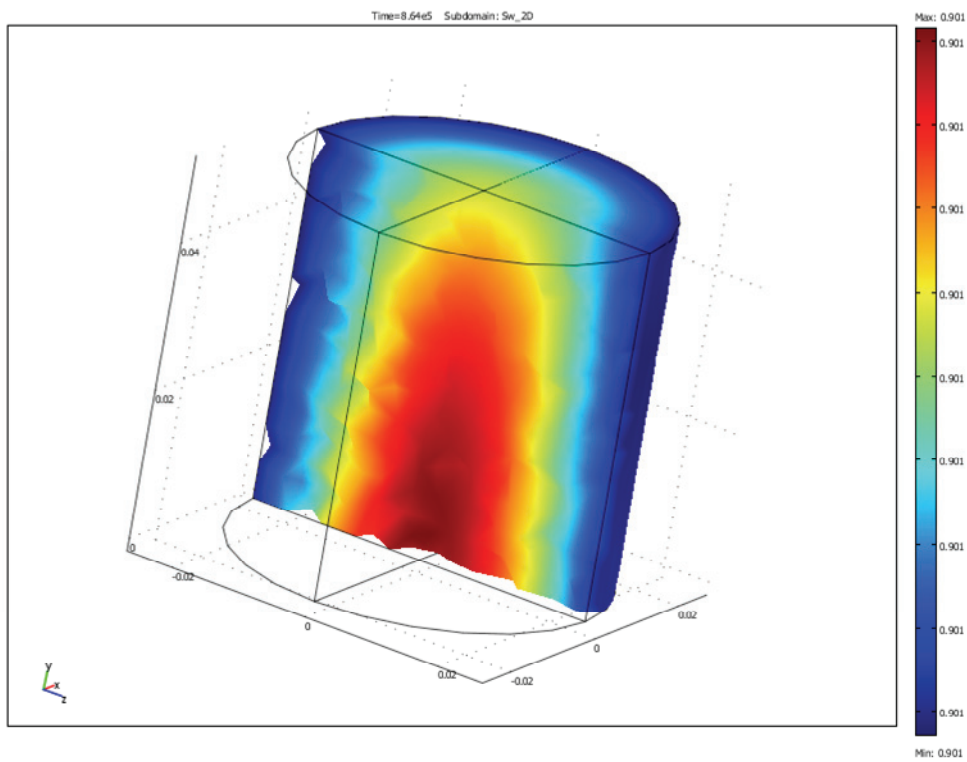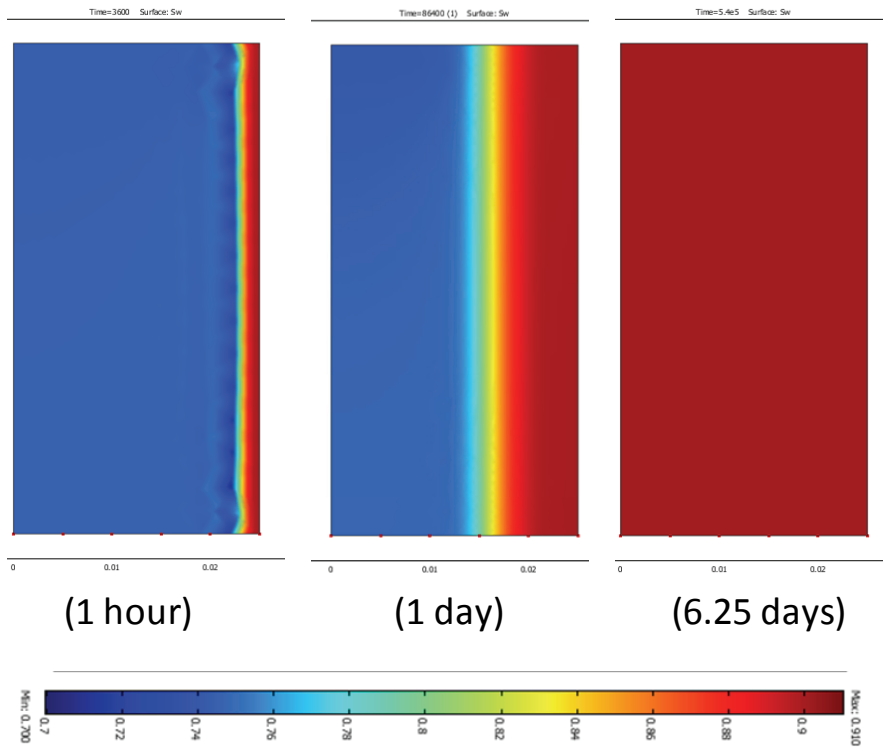
(10 days, with very small contour range)

Figure 38: Degree of Saturation Contour from COMSOL Analysis (Constant Mean Stress)
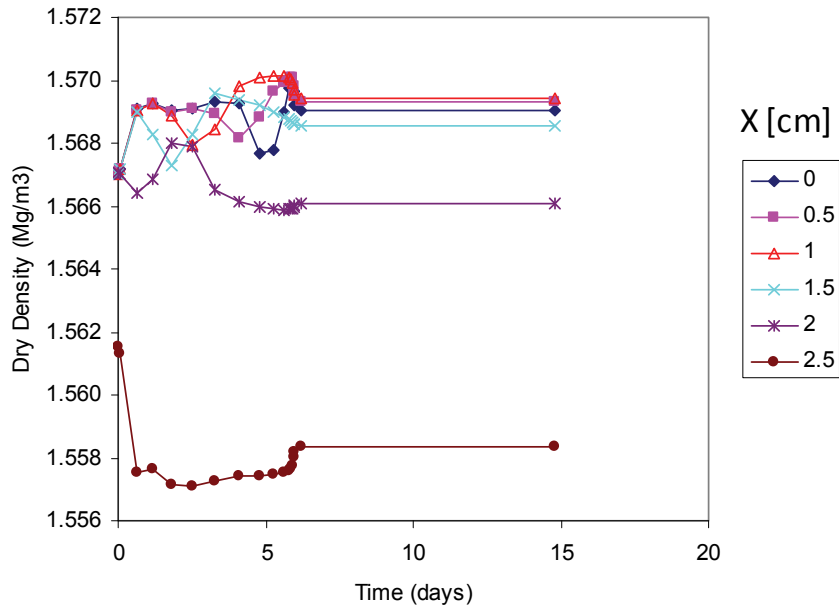
(a) CODE_BRIGHT
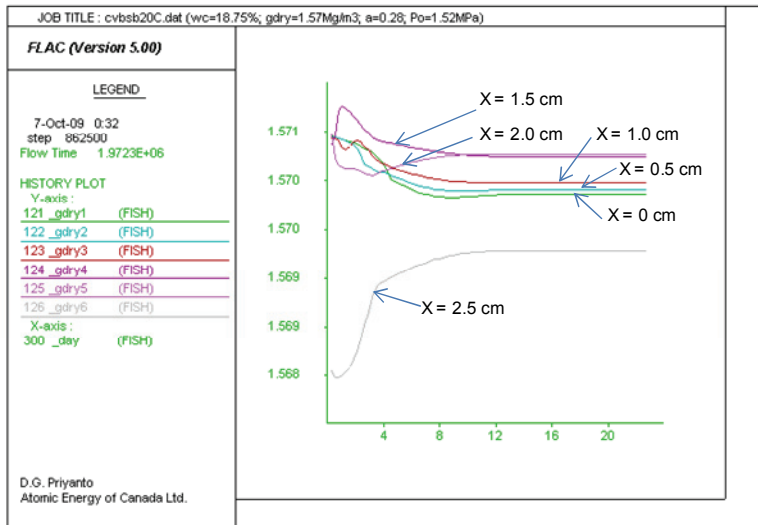
(b) FLAC-BSB Model
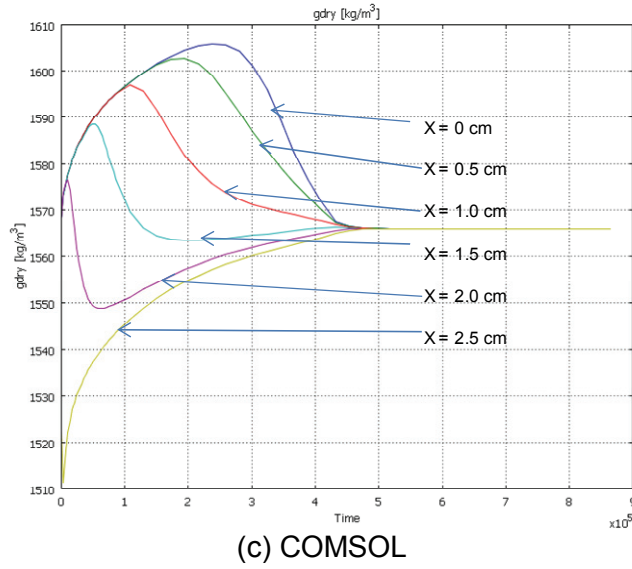
(c) COMSOL

Figure 39: Evolution of Dry Density (CV) (x is the radial distance refer to Figure 24a)

(a) CODE_BRIGHT
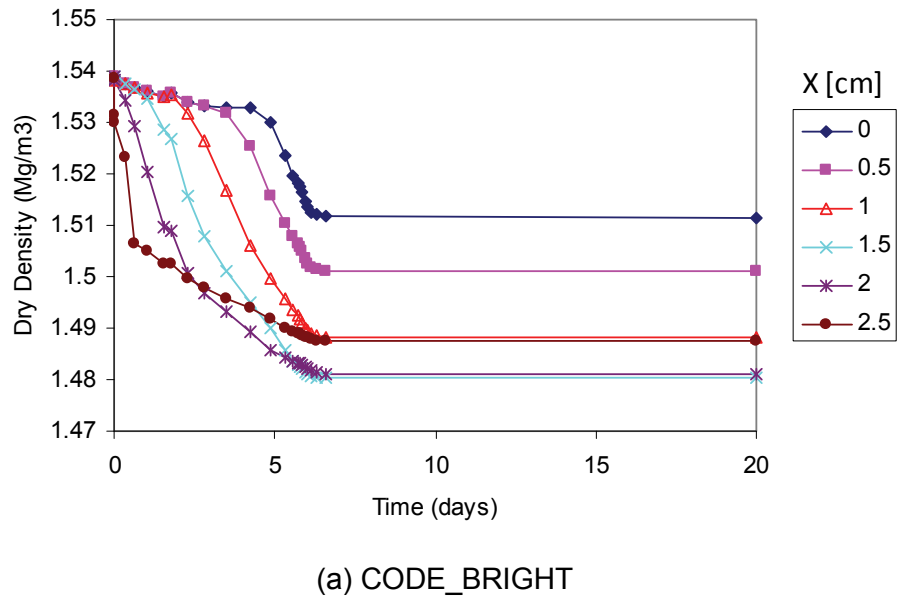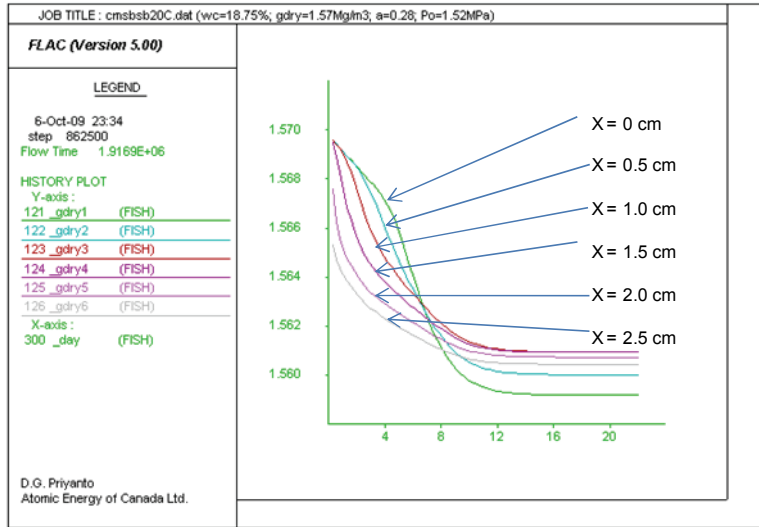
(b) FLAC-BSB Model
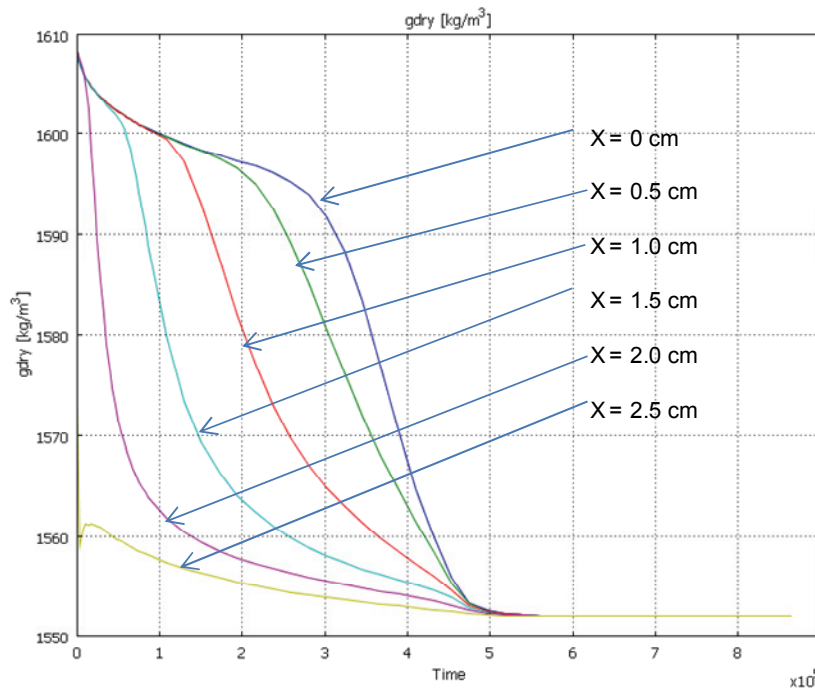
(c) COMSOL

Figure 40: Evolution of Dry Density (CMS) (x is the radial distance refer to Figure 24a)

6. SUMMARY AND CONCLUSION

This study has established a method for deriving the Hydraulic-Mechanical (HM) material properties and summarized parameters of elasto-plastic models and hydraulic constitutive models for unsaturated compacted bentonite-sand buffer (BSB) specimens.

This study utilized the existing constitutive models, including: original Basic Barcelona Model (BBM), van Genuchten (1980) model, and Kozeny's model. As observed in the laboratory test results of the BSB specimens, not all the features of the compacted BSB materials can be simulated using the existing constitutive models. This document has introduced three new constitutive models, including: the BBM-mod, BSB model and Smax model. The BBM-mod was similar to the original BBM, but uses Bishop's effective stress. The BSB model has the features observed in the laboratory tests of the BSB specimens, including M, κ, and λ as a function of S_e. The Smax model has S_{max} as a function of total porosity, based on the results of infiltration tests.

These parameters have been applied to simulate the infiltration process in triaxial specimens under constant volume (CV) and constant mean stress (CMS) tests using three different computer codes (i.e., CODE_BRIGHT, FLAC, and COMSOL). Eight HM analyses have been completed and the results were compared in order to examine the significance of many features of these models by comparing them to the results of laboratory tests. From these observations the following conclusions can be drawn:

- Compared to the analyses using one-phase flow formulation, two-phase flow formulation gave a smoother transition before and after equilibrium states, similar trend to the laboratory test results. Achieving equilibrium is indicated by achieving a no further change in the volume of water added to the specimen and constant suction.

- An elasto-plastic model results in variation of dry density at the end of test (equilibrium), similar trend to the laboratory test results.

- Variations of the coefficient of compressibility (κ) and critical state slope (M) have been observed from the laboratory triaxial test results for the bentonite-sand buffer (BSB) material for suction in the range of 0 to greater than 100 MPa. These features have been added in the numerical models using the BSB model. The numerical modelling of the infiltration triaxial test has shown that these features are not particularly important for the limited range of suction (approximately 0 to 3 MPa) investigated in this study. However, it may not be the case if the range of suction is substantial, similar to the range of laboratory test results.

- The Smax model can give a reasonable prediction of the total volume of water added to the specimen in the CV test, but not in the CMS test. It is expected due to the limitation of the linear elastic (LE) model used in the COMSOL model.

- Hydraulic and mechanical behaviour of the BSB specimens are related to each other. In order to match both magnitude and trend of the laboratory test data, it is necessary to include all the features of the BSB in one model simultaneously. Since none of the models presented in this document have included all these features simultaneously, it should be expected that none of the models provide good matches in both magnitude and trend with measured end of test saturation or dry density. CODE_BRIGHT and FLAC used elastoplastic model, but not the Smax model. COMSOL used the Smax model, but not the elastoplastic model.

- It is recommended that a means to incorporate the BSB model and Smax model simultaneously be developed in order to provide better matches between the numerical simulations and laboratory test measurements.

REFERENCES

Alonso, E.E., A. Gens and A. Josa. 1990. A constitutive model for partially saturated soils. Géotechnique, 40(3): 405-430.

Anderson, D.E.S. 2003. Evaluation and comparison of mechanical and hydraulic behaviour of two engineered clay sealing material. M.Sc Thesis, Dept. Civil Engineering, University of Manitoba, Winnipeg, Manitoba.

Baumgartner, P., D. Priyanto, J.R. Baldwin, J.A. Blatz, B.H. Kjartanson and H. Batenipour. 2008. Preliminary results of one-dimensional consolidation testing on bentonite clay-based sealing components subjected to two pore-fluid chemistry conditions. Nuclear Waste Management Organization Report NWMO TR-2008-04. Toronto, Canada.

Blatz, J.A. 2000. Elastic-plastic modelling of unsaturated high-plastic clay using results from a new triaxial test with controlled suction. Ph.D Thesis, Dept. Civil Engineering, University of Manitoba, Winnipeg, Manitoba.

Blatz, J.A. and J. Graham. 2000. A system for controlled suction in triaxial tests. Géotechnique, 50(4): 465-478.

Dixon, D.A. 1995. Towards an understanding of water structure and water movement through dense clays. Ph.D Thesis, Department of Civil and Geological Engineering, University of Manitoba, Winnipeg, Manitoba, Canada.

Gierszewski, P., J. Avis, N. Calder, A. D'Andrea, F. Garisto, C. Kitson, T. Melnyk, K. Wei and L. Wojciechowski. 2004. Third case study – Postclosure safety assessment. Ontario Power Generation, Nuclear Waste Management Division Report 06819-REP-01200-10109-R00. Toronto, Ontario.

Maak, P., and G.R. Simmons. 2005. Deep geologic repository concepts for isolation of used fuel in Canada. In Proc. Canadian Nuclear Society conference "Waste Management, Decommissioning and Environmental Restoration for Canada's Nuclear Activities: Current Practices and Future Needs". 2005 May 8-11, Ottawa.

Priyanto, D.G., J.A. Blatz, G.A. Siemens, R.B. Offman, J.S. Boyle and D.A. Dixon. 2008a. The effects of initial conditions and liquid composition on the one-dimensional consolidation behaviour of clay-based sealing materials. Nuclear Waste Management Organization Report NWMO TR-2008-06. Toronto, Canada.

Priyanto, D.G., J.A. Blatz, G.A. Siemens, R.B. Offman, J.S. Powell and D.A. Dixon. 2008b. The effects of fluid composition on the one-dimensional consolidation behaviour of clay-based sealing materials. Nuclear Waste Management Organization Report NWMO TR-2008-20. Toronto, Canada.

Roscoe, K.H., and J.B. Burland. 1968. On the generalized stress-strain behaviour of 'wet' clay. In J. Heyman and F. Leckie (Eds.), Engineering Plasticity (pp. 535-609). Cambridge: Cambridge University Press.

Russell, S.B. and G.R. Simmons. 2003. Engineered barrier system for a deep geologic repository. Presented at the 2003 International High-Level Radioactive Waste Management Conference. 2003 March 30-April 2, Las Vegas, NV.

Sheng, D., A. Gens, D.G. Fredlund and S.W. Sloan. 2008. Unsaturated soils: From constitutive modelling to numerical algorithms. Computers and Geotechnics 35 (2008): 810-824.

Siemens, G.A. 2006. Influence of boundary conditions on the hydraulic-mechanical behaviour of an unsaturated swelling soil. Ph.D Thesis, Dept. Civil Engineering, University of Manitoba, Winnipeg, Manitoba.

Tang, G.X. 1999. Suction characteristics and elastic-plastic modelling of unsaturated sand-bentonite mixture. Ph.D Thesis, Dept. Civil Engineering, University of Manitoba, Winnipeg, Manitoba.

van Genuchten, M.T. 1980. A closed form equation for predicting the hydraulic conductivity of unsaturated soils. Soil Sc. Soc. Am. J. 44, 892-898.

Wiebe, B.J. 1996. The effect of confining pressure, temperature, and suction on the strength and stiffness of unsaturated buffer. M.Sc. Thesis, Department of Civil and Geological Engineering, University of Manitoba, Winnipeg, MB.